

## Reply to reviewers

acp-2014-970

### Chemical characterization of submicron regional background aerosols in the Western Mediterranean using an Aerosol Chemical Speciation Monitor

Please find below a detailed reply to each of the comments. A new version of the manuscript has been prepared accordingly.

Most of the further comments from Referee 1 have been addressed. To further improve the clarity of the manuscript, I suggest the following information to be included:

1. An unexplained mass of 7% for the warmer period is fairly large. More details on the residuals should be provided for both the warm period and the cold period for the readers to gain a better understanding of the residuals. Please at least include these plots, 1)  $Q/Q_{exp}$  vs. number of factors, 2) Distribution of scaled residuals for each  $m/z$ , 3) Time series of the measured and the reconstructed organic mass, 4)  $Q/Q_{exp}$  vs. time, 5)  $Q/Q_{exp}$  vs.  $m/z$ .

The unexplained mass for the warmer period is actually only 2%. There was a mistake in the previous calculation (a problem with the averaging periods). We apologize for this mistake, which has been corrected in the revised manuscript.

Please find the requested plots below for both warm and cold periods. The plots have been added to the supplementary information and referenced in the revised manuscript:

1)  $Q/Q_{exp}$  vs number of factors:

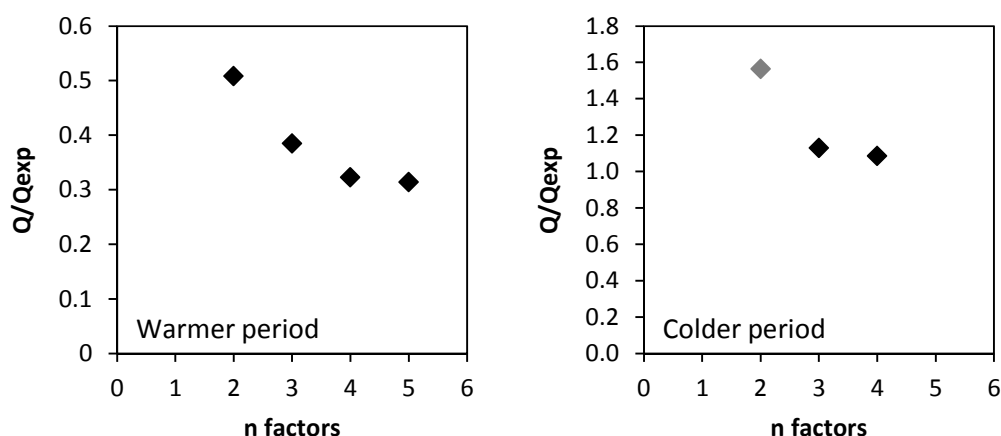


Figure S11.  $Q/Q_{exp}$  vs number of factors for the warmer and the colder periods. The grey dot in the colder period corresponds to a solution with an  $a$ -value of 0.2 for the BBOA factor, given that there was no convergence with an  $a$ -value of 0.1 for the 2-factors solution.

2) Distribution of scaled residuals for each  $m/z$ :

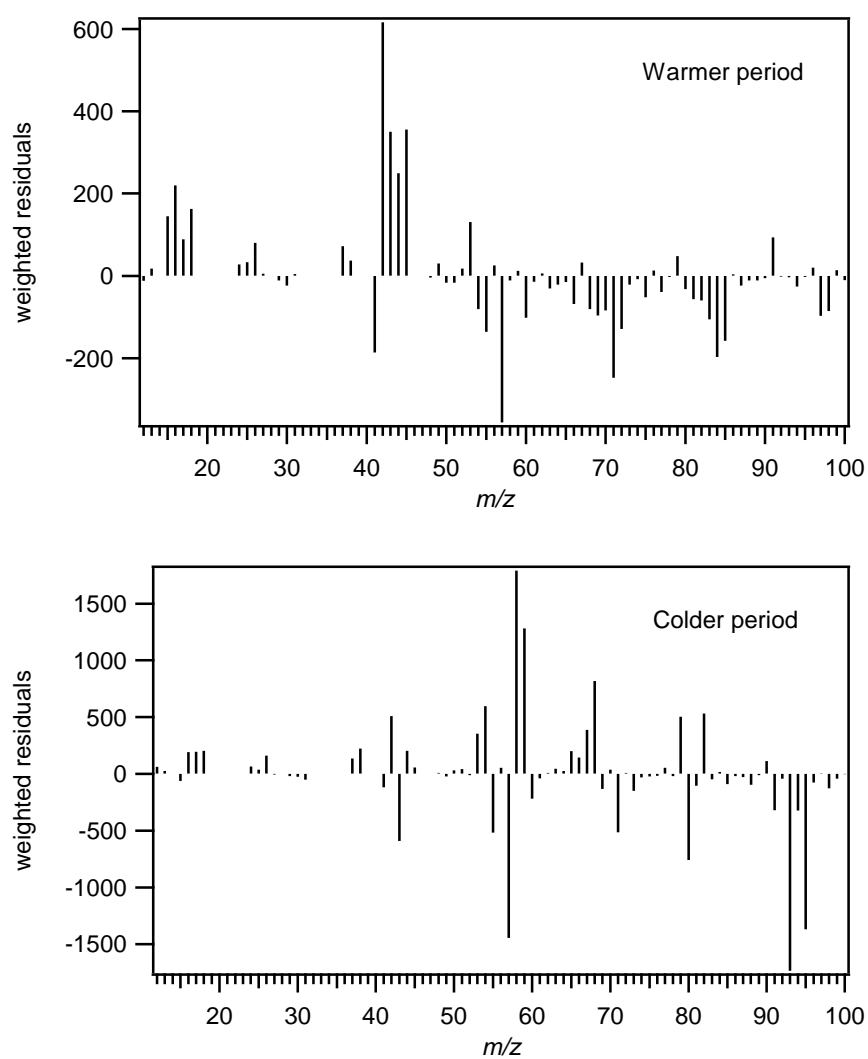


Figure S12. Weighted residuals vs  $m/z$  for the warmer and the colder periods.

3) Time series of the measured and the reconstructed organic mass:

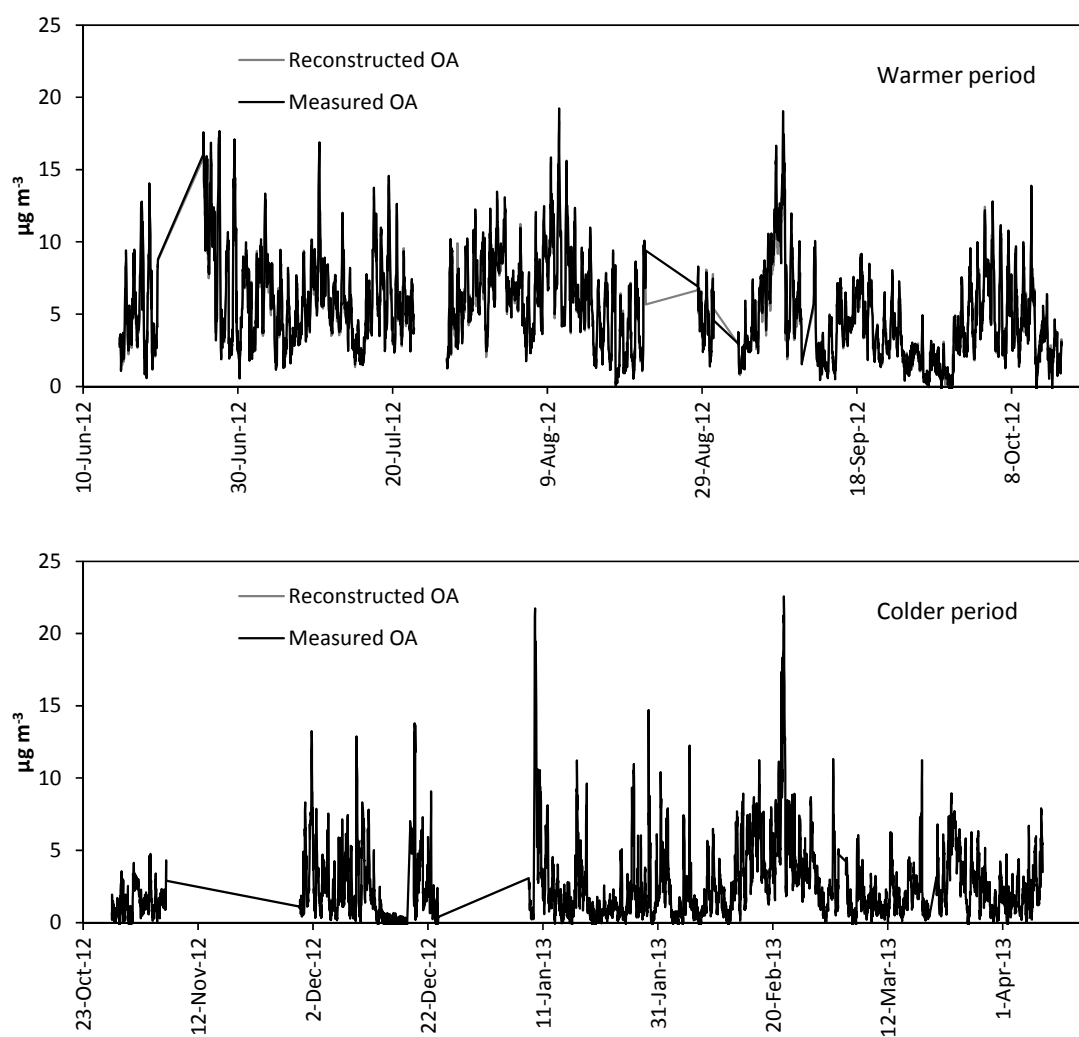


Figure S13. Time series of the measured and reconstructed OA concentrations for the warmer and the colder periods.

4)  $Q/Q_{exp}$  vs time:

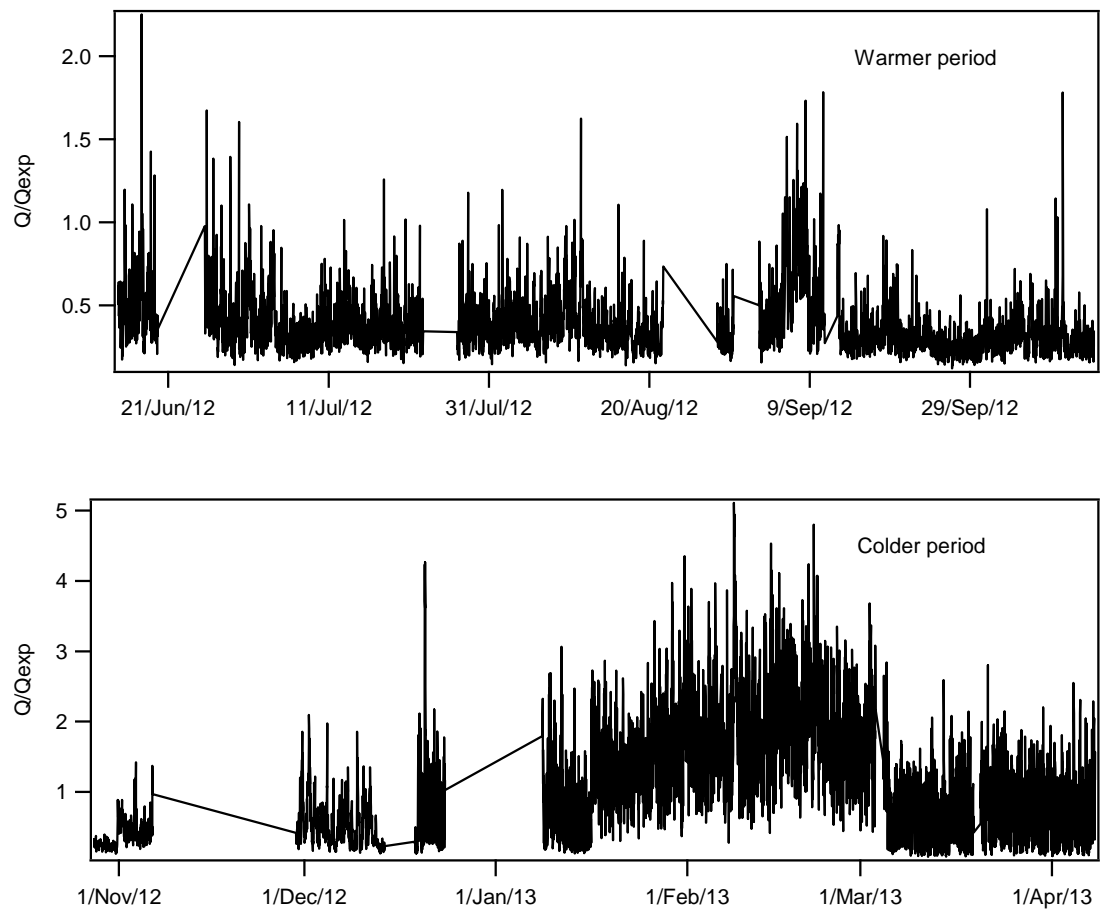


Figure S14. Time series of  $Q/Q_{exp}$  for the warmer and the colder periods.

5)  $Q/Q_{exp}$  vs  $m/z$ :

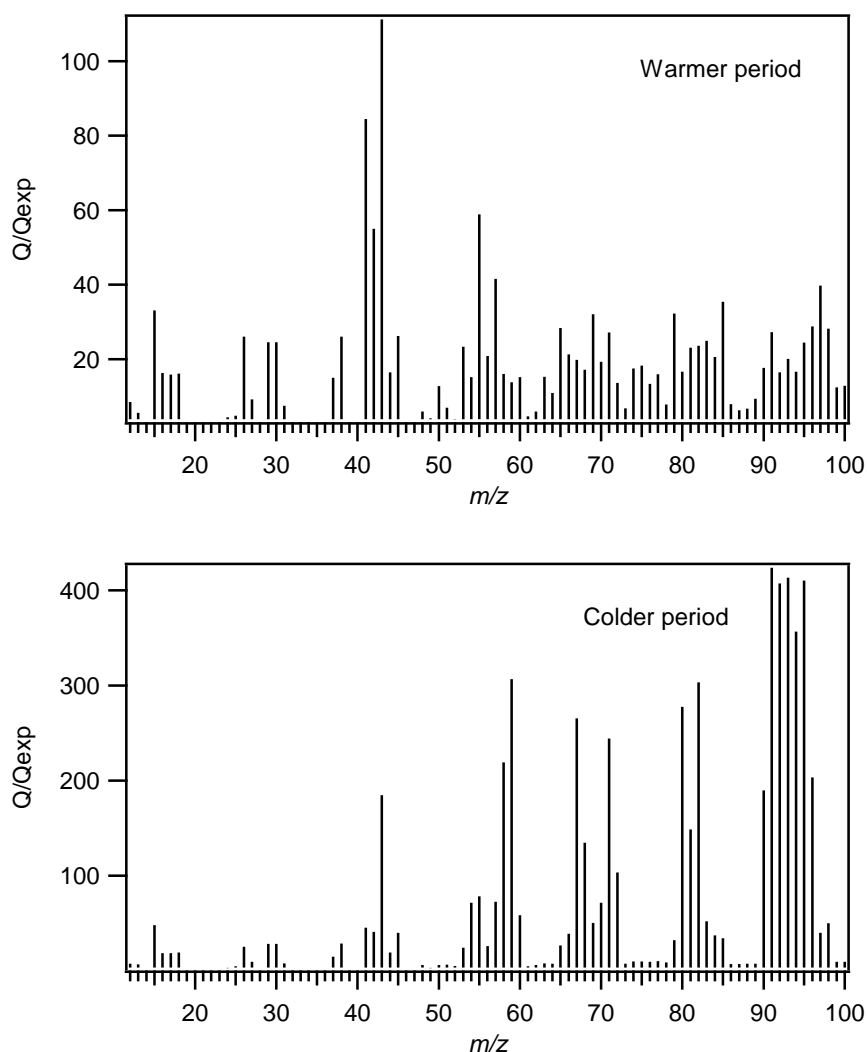


Figure S15.  $Q/Q_{exp}$  vs  $m/z$  for the warmer and the colder periods.

**2. Are the rotational ambiguity of the solutions and the robustness of the solutions explored with the use of FPEAK and SEED parameters? If so, please provide relevant discussions/results. If not, please explain why these are not examined.**

We did not explore the degree of rotational ambiguity within the fpeak methodology, since it leads to a lower estimate of the rotational uncertainty only. All runs with unconstrained information in G and F were always initialized with random entries and hence the seed exploration was done within these runs. In addition, a more specific exploration of the solution space was performed within the a-value approach that investigated the relaxation of constrained anchor profiles to the PMF input data.

3. In the response, the authors have provided further info regarding the correlations ( $R^2$  values) of PMF factors with external tracers. Currently, these values are included in the text here and there. In order to offer a clearer overview of these correlations for the readers, please provide a summary figure (or table) in the SI showing the correlations of each PMF factor with all the external tracers considered. Please do so for both the summer data and winter data. As the authors suggested that the specific characteristics of Montseny might lead to better (or worse) correlations of some PMF factors with certain external tracers, these summary correlation figures would be useful references for future studies in the area.

A table summarizing all the squared Pearson correlation coefficients has been added to the supplementary material and is referenced in the revised manuscript.

**Table S1. Squared Pearson correlation coefficients between OA sources/types and BC, sulphate, nitrate and ammonium for the warmer and the colder periods.**

$R^2$		BC	SO <sub>4</sub>	NO <sub>3</sub>	NH <sub>4</sub>
Warmer period	HOA	0.51	0.16	0.23	0.16
	SV-OOA	0.32	0.17	0.16	0.13
	LV-OOA	0.45	0.34	0.27	0.43
Colder period	HOA	0.70	0.20	0.53	0.49
	BBOA	0.66	0.21	0.49	0.47
	OOA	0.71	0.49	0.73	0.79

Once these are included in the revised manuscript/SI, the manuscript will be acceptable for publication in ACP.

**Chemical characterization of submicron regional background aerosols in the Western  
Mediterranean using an Aerosol Chemical Speciation Monitor**

M.C. Minguillón<sup>1</sup>, A. Ripoll<sup>1,2</sup>, N. Pérez<sup>1</sup>, A.S.H. Prévôt<sup>3</sup>, F. Canonaco<sup>3</sup>, X. Querol<sup>1</sup>, A. Alastuey<sup>1</sup>

<sup>1</sup>Institute of Environmental Assessment and Water Research (IDAEA-CSIC), Jordi Girona 18-26,  
Barcelona, 08034, Spain

<sup>2</sup>Departament d'Astronomia i Meteorologia, Universitat de Barcelona, Martí i Franquès 1,  
08028, Barcelona, Spain

<sup>3</sup>Paul Scherrer Institute, Laboratory of Atmospheric Chemistry, 5232 Villigen PSI, Switzerland

\*Corresponding author: mariacruz.minguillon@idaea.csic.es

**ABSTRACT**

An Aerosol Chemical Speciation Monitor (ACSM, Aerodyne Research Inc.) was deployed at Montseny (MSY, 720 m a.s.l.) regional background site in the Western Mediterranean from June 2012 to July 2013 to measure real-time inorganic (nitrate, sulphate, ammonium and chloride) and organic submicron aerosol concentrations. Co-located measurements were also carried out including real-time submicron particulate matter (PM<sub>1</sub>) and black carbon (BC) concentrations, and off-line PM<sub>1</sub> chemical analysis. This is one of the few studies that compare ACSM data with off-line PM<sub>1</sub> measurements, avoiding the tail of the coarse mode included in the PM<sub>2.5</sub> fraction. The ACSM + BC concentrations agreed with the PM<sub>1</sub> measurements, and strong correlation was found between the concentrations of ACSM species and the off-line measurements, although some discrepancies remain unexplained. Results point to a current underestimation of the relative ionization efficiency (RIE) established for organic aerosol (OA), which should be revised in the future. The OA was the major component of submicron aerosol (53% of PM<sub>1</sub>), with a higher contribution in summer (58% of PM<sub>1</sub>) than in winter (45% of PM<sub>1</sub>). Source apportionment of OA was carried out by applying Positive Matrix Factorization (PMF) using the Multilinear Engine (ME-2) to the organic mass spectral data matrix. Three sources were identified in summer: hydrocarbon-like OA (HOA), low-volatile oxygenated OA (LV-OOA), and semi-volatile oxygenated OA (SV-OOA). The secondary OA (SOA, 4.8 µg m<sup>-3</sup>, sum of LV-OOA and SV-OOA) accounted for 85% of the total OA and its formation during daytime (mainly SV-OOA) was estimated to be 1.1 µg m<sup>-3</sup>. In winter, HOA was also identified (12% of OA), a contribution from biomass burning OA was included, and it was not possible to differentiate two different SOA factors but a single OOA factor was resolved. The OOA contribution represented the 60% of the total OA, with a degree of oxidation higher than both OOA summer factors. An intense wildfire episode was studied obtaining a region-specific BBOA profile.

**KEYWORDS:** ACSM, PM<sub>1</sub>, organics, chemical composition, Mediterranean, air quality.

Eliminado: 7



## 1 INTRODUCTION

Ambient aerosols have adverse effects on human health (Pope III and Dockery, 2006), and affect climate (IPCC, 2013), ecosystems, crops, and regional visibility. Fine particulate matter ( $PM_{10}$ , particles with an aerodynamic diameter  $<10 \mu m$ ) contains substantial fractions of inorganic compounds and carbonaceous aerosols, the latter reaching up to 90% of the mass (Jimenez et al., 2009). Carbonaceous aerosols are comprised of organic compounds, collectively referred to as organic aerosol (OA), elemental carbon (EC), and carbonates (from mineral dust), although the latter can be considered negligible in submicron aerosols.

The Western Mediterranean Basin (WMB) has special atmospheric and geographic characteristics that imply the interest of the detailed study of the ambient aerosols in this area (Querol et al., 2009). The regional background has been investigated through long data series of measurements in previous studies available at Montseny (representative of the regional background in the WMB). Pérez et al. (2008) found average particulate matter concentrations at Montseny of 17, 13 and  $11 \mu g m^{-3}$  of  $PM_{10}$ ,  $PM_{2.5}$  and  $PM_{10-2.5}$ , respectively, in the 2002-2007 period. Cusack et al. (2012) and Querol et al. (2014) found a decreasing trend in  $PM_{2.5}$  concentrations from 2001 to 2012 of  $-0.39 \mu g m^{-3}$  per year.  $PM_{2.5}$  concentrations were found higher in the WMB than at other rural background sites across Spain, Portugal, Germany and Scandinavia but lower than those measured in Switzerland, Italy and Austria (Cusack et al., 2012). The prevailing daily evolution is driven by the breeze circulation (mountain and sea breezes), with lower  $PM_x$  concentrations at night owing to the nocturnal drainage flows, and higher  $PM_x$  concentrations at midday owing to the transport of atmospheric pollutants accumulated in the pre-coastal depression upwards by the breeze (Pérez et al., 2008). Maximum  $PM_{10}$  concentrations were found in summer, February-March and November, and sporadic  $PM_x$  increases may be recorded under anticyclonic conditions (Pey et al., 2010). The chemical composition of  $PM_{2.5}$  is characterised by high concentrations of organic aerosol and sulphate, followed by crustal material, nitrate and ammonia, with sea spray and elemental carbon being a minor part of the total  $PM_{2.5}$  mass (Cusack et al., 2012). Compared to other central European sites, the Western Mediterranean aerosol is characterised by higher concentrations of crustal material but lower concentrations of organic aerosol, elemental carbon and ammonium nitrate (Pey et al., 2009). Nevertheless, relatively high  $PM_{2.5}$  concentrations of carbonaceous aerosol and sulphate transported from populated coastal areas are regularly recorded, especially during winter anticyclonic episodes and summer midday PM highs (Pey et al., 2009; Pey et al., 2010). A organic carbon (OC) to elemental carbon (EC) ratio (14 in summer, 10 in winter) was detected, pointing to the influence of biogenic

Código de campo cambiado

emissions, secondary organic aerosol (SOA) formation favoured by high ozone concentrations and insolation, and intensive recirculation of aged air masses (Pey et al., 2009; Querol et al., 2013).

The sources of organic aerosol in the regional background site of Montseny were studied in two intensive campaigns, using off-line  $^{14}\text{C}$  analysis (Minguillón et al., 2011), Aerosol Mass Spectrometers (AMS) (Minguillón et al., 2011; Crippa et al., 2014), and organic tracers (Alves et al., 2012; Van Drooge et al., 2012). Minguillón et al. (2011) found that the contribution of fossil fuel combustion sources (mainly road traffic emissions) to OC at Montseny was 31% and 25%, in winter and summer, respectively, and that 85% of this fossil OC was secondary. The contribution of biomass burning emissions was relatively low when compared with other regional background sites in Europe, and was estimated to be 21% and 12% of the total OC in winter and summer, respectively. Alves et al. (2012) concluded that the anthropogenic input may be associated with the transport of aged air masses from the surrounding industrial/urban areas, which superimpose the locally originated biogenic hydrocarbons.

Besides these studies, a long time series of organic aerosol data has not been analysed in Montseny. To this end, the newly-developed Aerosol Chemical Speciation Monitor (ACSM) would be suitable (Ng et al., 2011b), as opposed to the use of AMS, which cannot work unattended and therefore is usually employed around the world for periods of about one month. Nevertheless, due to its recent implementation, some studies based on ACSM data are found in the literature (Ng et al., 2011b; Shaw et al., 2012; Sun et al., 2012; Budisulistiorini et al., 2013; Canonaco et al., 2013; Carbone et al., 2013; Sun et al., 2013a; Sun et al., 2013b; Takahama et al., 2013; Bougiatioti et al., 2014; Canonaco et al., 2014; Petit et al., 2014; Ripoll et al., 2014a).

The present study aims at interpreting a one-year time series of inorganic and organic compounds in the submicron aerosol in the regional WMB, with special focus on their evolution throughout the year as a function of the concatenation of different atmospheric scenarios. The different types and origin of organic aerosol (OA) are also investigated. To this end, an ACSM was deployed for a year in the regional background site of Montseny (MSY), according to the schedule planned within the Aerosols, Clouds, and Trace gases Research InfraStructure (ACTRIS) Network project. Moreover, a validation of the ACSM data is carried out by comparison with co-located instruments both real-time and off-line.

## 2 METHODOLOGY

### 2.1 Sampling site

The MSY station (41°46'46"N, 02°21'29"E, 720 m a.s.l.) is located in the Montseny natural park, in a densely forested area, 50 km to the N-NE of the Barcelona urban area, and 25 km from the Mediterranean coast. The station is located on the upper walls of a valley extending perpendicularly from the Catalan Pre-Coastal ranges to the coast. The site is relatively far from urban and industrial areas, but it can be affected by anthropogenic emissions transported from populated and industrialised areas under specific meteorological conditions. The MSY station is in the ACTRIS Network (formerly EUSAAR, European Supersites for Atmospheric Aerosol Research), is a Global Atmosphere Watch (GAW) site, and is part of the IDAEA-CSIC and the Department of Environment of the Autonomous Government of Catalonia air quality monitoring network.

The prevailing atmospheric dynamics has been described elsewhere (Pérez et al., 2008; Pey et al., 2009). Briefly, in winter the location of the Azores high pressure system favours the entry of clean Atlantic air masses into the WMB which replace the existing air masses leading to a decrease of pollutants. In summer, the very weak pressure gradients result in local circulations dominating the atmospheric dynamics with the consequent accumulation of pollutants (Millán et al., 1997). The climate is typical Mediterranean with warm summers, temperate winters and irregular precipitation rates during the year.

The daily classification of meteorological episodes affecting MSY during the study period was made as described in Pérez et al. (2008), leading to the following types of scenario: Atlantic Advection, North African, Mediterranean, European, Regional, and Winter Anticyclonic Episodes. The frequency of each type of scenario for each of the months of the study period is shown in [Figure S1](#).

Eliminado: Figure S1

### 2.2 ACSM settings, calibrations and data processing

An ACSM was deployed from June 2012 to July 2013, according to the ACTRIS schedule, to measure non-refractory submicron aerosol species (organics, nitrate, sulphate, ammonium and chloride) in real-time (Ng et al., 2011b). Briefly, the instrument uses an aerodynamic lens to sample and focus submicron particles (75-650 nm) into a narrow particle beam (Liu et al., 2007), with a flow of approximately 85 cc/min. The beam is transmitted into the final of three vacuum chambers, where particulate matter is flash-vaporized on a hot oven (600 °C), ionized by hard electron impact ionization (70eV) and subsequently detected using a

commercial quadrupole mass spectrometer. The concentration of the aforementioned species is calculated based on the measured aerosol mass spectra. For a given species, its concentration is calculated based on the addition of the ion signals at each of its mass spectral fragments and its ionization efficiency (IE) (Canagaratna et al., 2007). Since calibration of IEs for all ambient species is not feasible, the relative ionization efficiency (RIE) (compared to that of nitrate) is used for different species.

Thus, mass calibration of the ACSM is based on determining the instrument response factor (RF) using ammonium nitrate calibration aerosol (Ng et al., 2011b). In this study, an atomizer (TSI, Constant Output Atomizer Model 3076) was used for primary aerosol generation, followed by a silica gel diffusion dryer, an SMPS system (model TSI 3936), comprised of an electrostatic classifier (model TSI 3080) with a differential mobility analyzer (DMA, model TSI 3081) and a condensation particle counter (CPC, TSI 3772). Monodisperse 300 nm ammonium nitrate aerosol particles were generated for the calibration. The calibration comprised a range of nitrate concentrations from 0 to 15  $\mu\text{g m}^{-3}$ , which were achieved by diluting the generated aerosol. RIE for ammonium was directly determined from the ammonium nitrate calibration.

Several calibrations were carried out through the sampling period, and average values for nitrate IE and RIE for ammonium were used for the whole dataset. After several tests around the world, more experience has been gained regarding the performance of the ACSM. Hence, RIE for sulphate has been shown to vary from instrument to instrument and therefore the default value (1.2) (Ng et al., 2011b) cannot be directly used. Nevertheless, this information was known when our ACSM was no longer at the MSY station, and hence, sulphate RIE was determined by doing the aforementioned calibration exercise with ammonium sulphate monodisperse aerosol in Barcelona. The sulphate RIE value found was very close to the default value and hence 1.2 was used for the current dataset. The default RIE for organics (1.4) (Ng et al., 2011b) has been used, although some discussion about this can be found in section 3.1.

The ACSM was connected to a general inlet equipped with a nafion drier to maintain the RH below 40%, although technical problems resulted in some periods (about 50% of the data points) with uncontrolled RH. The ACSM was set to measure with a time resolution of approximately 30 minutes, resulting from setting it to work with 24 scans (alternatively 1 sample and 1 filtered) per data point with a scan speed of 500 ms/amu. The data acquisition software provided by Aerodyne Research (version 1.4.2.5 from the beginning to 18<sup>th</sup> December 2012, and version 1.4.3.8 for the rest of the period) was used to process the measurements. The data were analyzed with the ACSM data analysis software version 1.5.3.2 (Aerodyne

Research Inc.) written in Igor Pro (WaveMetrics, Inc., Lake Oswego, OR, USA). A correction for the instrument performance limitations was applied to the dataset based on the inlet pressure and N<sub>2</sub> signal. The aerosol mass concentrations were then corrected for particle collection efficiency (CE) following the Middlebrook approach (Middlebrook et al., 2012). The aerosols at MSY are assumed to be internally mixed and thus the CE was assumed to be the same for different components in contrast to e.g. Hawkins et al. (2010).

### 2.3 Additional measurements and instrumentation

Submicron particulate matter (PM<sub>1</sub>) 24-h samples were collected on quartz fibre filters (Pallflex 2500QAT-UP) using DIGITEL (DH-80) high volume (30 m<sup>3</sup> h<sup>-1</sup>) samplers with a PM<sub>1</sub> impactor inlet. The sampler, and therefore the collected samples, was kept inside a container with controlled temperature (between 24 and 26°C). Samples were collected every 4 days. Gravimetric PM<sub>1</sub> determination was carried out by weighing the filters before and after sampling, after stabilization in a conditioned room (20°C and 50% relative humidity). Chemical off-line analyses were carried out. A quarter of the filter was acid digested (HNO<sub>3</sub>:HF:HClO<sub>4</sub>), and the resulting solution was analysed by Inductively Coupled Plasma Atomic Emission Spectroscopy (ICP-AES) for major elements determination, including S, from which the sulphate concentration was calculated. Another quarter of the filter was water extracted to determine the nitrate, sulphate and chloride concentrations by Ion Chromatography and the ammonium concentrations by an ion selective electrode. OC concentrations were determined by thermal-optical methods using a Sunset instrument following the EUSAAR2 thermal protocol (Cavalli et al., 2010). Blank filters were analysed together with the samples and concentrations were subtracted from those found in the samples in order to calculate the ambient concentrations.

PM<sub>1</sub> hourly concentrations were measured using an optical particle counter (GRIMM, model 180) and corrected with the simultaneous 24-h gravimetric measurements (Alastuey et al., 2011). Equivalent Black Carbon (BC) mass concentrations (Petzold et al., 2013) were measured with a 1-minute time resolution by a multi-angle absorption photometer (MAAP, model 5012, Thermo) using a PM<sub>10</sub> inlet, and using the default mass absorption cross section (MAC) from the instrument software (6.6 m<sup>2</sup> g<sup>-1</sup>). Particle number size distributions (9-820 nm) were measured by a Scanning Mobility Particle Sizer (SMPS), comprising a DMA connected to a CPC (TSI 3772), with a system designed and manufactured at the Leibniz Institute for Tropospheric Research (Wiedensohler et al., 2012). The mass concentration from SMPS data

was calculated from the total volume of particles and the composition-dependent density calculated based on the ACSM chemical composition.

Wind direction and speed, solar radiation, temperature, relative humidity and precipitation were recorded using conventional instruments and hourly data can be seen in

Figure S2,

Eliminado: Figure S2

## 2.4 Source apportionment of OA

The source apportionment to the organic fraction can be investigated by applying Positive Matrix Factorization (PMF) (Paatero and Tapper, 1994) using the Multilinear Engine (ME-2) (Paatero, 1999) to the organic mass spectra. Both methods describe the measurements with a bilinear factor model:

$$x_{ij} = \sum_{k=1}^p g_{ik} f_{kj} + e_{ij} \quad (1)$$

where  $x_{ij}$  is the  $j^{\text{th}}$  species ( $m/z$ ) concentration measured in the  $i^{\text{th}}$  sample,  $p$  is the number of sources,  $g_{ik}$  is the contribution of the  $k^{\text{th}}$  source to the  $i^{\text{th}}$  sample,  $f_{kj}$  is the concentration of the  $j^{\text{th}}$  species in the  $k^{\text{th}}$  source (mass spectra) and  $e_{ij}$  is the residual associated with the  $j^{\text{th}}$  species concentration measured in the  $i^{\text{th}}$  sample. The values  $g_{ik}$  and  $f_{kj}$  are adjusted until a minimum for the objective function  $Q$  for a given number of factors  $p$  is found:

$$Q = \sum_{i=1}^n \sum_{j=1}^m \left( \frac{e_{ij}}{\sigma_{ij}} \right)^2 \quad (2)$$

where  $\sigma_{ij}$  is the user defined uncertainty for the  $j^{\text{th}}$  species in the  $i^{\text{th}}$  sample.

With the ME-2, the user can introduce a priori information about sources e.g. using the so-called a-value approach. Hence, the user inputs one or more factor profiles and a constraint defined by the a-value, which determines the extent to which the output profile can differ from the profile fed to the model.

In the present study the source apportionment to OA was performed applying ME-2 using the toolkit SoFi (Source Finder) version 4.7 described in Canonaco et al. (2013). The ME-2 was applied separately for the warm and cold periods in this study, given the expected differences among them. The warm period was defined as a period with >70% of the days with average  $T > 19^{\circ}\text{C}$ , hourly max  $T > 24^{\circ}\text{C}$  and hourly min  $T > 15^{\circ}\text{C}$ , which includes 14<sup>th</sup> June to 9<sup>th</sup> October 2012. The cold period was defined as a period with >70% of the days with average  $T < 10^{\circ}\text{C}$ , hourly max  $T < 13^{\circ}\text{C}$  and hourly min  $T < 8^{\circ}\text{C}$  and includes 28<sup>th</sup> October 2012 to 7<sup>th</sup> April 2013. Only  $m/z \leq 100$  were used for several reasons: a) the signals of  $m/z > 100$  account for a

minor fraction of the total signal (2% on average), b) the  $m/z > 100$  have larger uncertainties, and c) the large interference of naphthalene signals (at  $m/z$  127, 128, and 129) is avoided. The error matrix was calculated by the aforementioned customized software, which downweights the  $m/z$  masses calculated from the  $m/z$  44 signal. Moreover,  $m/z$  with signal to noise ratio (S/N) below 0.2 were downweighted by a factor of 10, and those with S/N between 0.2 and 1 were downweighted by a factor of 2.

### 3 RESULTS AND DISCUSSION

#### 3.1 Comparison of ACSM data with other measurements

This is one of the few studies, together with Ripoll et al. (2014a), that compare ACSM data with off-line  $PM_{10}$  measurements. Most of the studies found in the literature comparing ACSM data with off-line measurements are based in the  $PM_{2.5}$  fraction for the off-line measurements. In this study we use  $PM_{10}$  measurements, avoiding the tail of the coarse mode that the  $PM_{2.5}$  fraction includes, and hence being closer to the size range measured by the ACSM (75-650nm).

The sum of the ACSM components concentrations and the BC concentrations measured by the MAAP was compared with  $PM_{10}$  concentrations determined by the optical particle counter, resulting in a strong correlation (squared Pearson correlation coefficient,  $R^2=0.66$ ) and a slope very close to unity (1.005) (Figure 1). The application of a time-dependent collection efficiency (CE) to the ACSM data based on the Middelbrook approach (Middlebrook et al., 2012) resulted in a better fit compared to the use of a constant  $CE=0.5$  used in several studies (which resulted in a slope of 0.913 and a  $R^2=0.65$ ). Hence the time-dependent CE application is considered more suitable for the present study. The time-dependent CE equalled the default value of 0.45 for most of the period, and increased up to 0.65 during the colder period (Figure S3). The sum of ACSM components and BC concentrations was also compared to the mass concentration calculated from SMPS data, resulting in a strong correlation (squared Pearson correlation coefficient,  $R^2=0.77$ ) and a slope very close to unity (0.997) (Figure S4). Moreover, ACSM components concentrations were daily averaged and compared to off-line measurements from 24-h  $PM_{10}$  samples (Figure 2). All the species, except for chloride, showed strong correlations ( $R^2$  of 0.68, 0.82 and 0.94 for ammonium, nitrate and sulphate, respectively). Chloride concentrations were below or close to detection limits for both ACSM and off-line analysis, which may be the cause for the discrepancies found. Such discrepancies were also found in other studies (Budisulistiorini et al., 2014). For the strongly-correlated

Código de campo cambiado

Eliminado: Figure 1

Eliminado: Figure S3

Eliminado: Figure S4

Eliminado: Figure 2

Código de campo cambiado

species, the slopes (ACSM vs off-line measurements) were different for each of them. Whereas it was close to unity for sulphate (1.15), it was higher for ammonium (1.72), and much higher for nitrate (2.80). The final reasons for this discrepancy remain unexplained, although a possible cause is the volatilization of ammonium nitrate from the filters. Nevertheless, the volatilization of ammonium nitrate is expected to be low given that the samples are kept at controlled conditions (24-26°C) as described in the methods section. Moreover, if random volatilization occurred, the correlation coefficients found between ACSM and filters would be lower. The apparent discrepancy between the slope for total PM<sub>1</sub> (ACSM+BC vs PM<sub>1</sub> from OPC corrected with gravimetric measurements, close to unity) and the slopes for the different components (>1) is attributed to the undetermined fraction of PM<sub>1</sub> mass in the filters. Thus, whereas the ACSM+BC concentrations are strictly the sum of the components, the PM<sub>1</sub> gravimetric concentrations include a fraction of undetermined mass, partially attributed to water (Figure S5).

For organic aerosol a strong correlation was found ( $R^2=0.82$ ), and the high slope obtained (4.25) may be interpreted as the OM-to-OC ratio, since the ACSM measures OA and the off-line measurements determined OC. This large OM-to-OC ratio suggests photochemically well-aged organics, but it is too high even for a pure SOA (Aiken et al., 2008), which is expected to have an important contribution at MSY as will be discussed later (section 3.5), and it is higher than the OM-to-OC ratio determined in March 2009 at Montseny (2.0) (Minguillón et al., 2011). This extremely large OM-to-OC ratio might be attributed to a) underestimation of OC due to loss of semi-volatile organic compounds from the filters, and b) overestimation of OM by the ACSM due to an underestimation of the RIE for organics. The first reason is expected to be less likely given the strong correlation found between OA and OC (which would not be so if random volatilization occurred) and given that the samples are kept at controlled conditions, as formerly explained, hence reducing the possible volatilization. Previous studies also found higher than expected OM-to-OC ratios when comparing ACSM OA with off-line OC measurements. Budisulistiorini et al. (2014) found OM-to-OC ratios of 4.85 and 3.85 in summer and fall, respectively. Ripoll et al. (2014a) found an OM-to-OC ratio of 3.39 for a one year sampling period. This topic is currently being investigated by the ACSM manufacturer. The calculation of OM-to-OC ratio from the f44 based on Aiken et al. (2008) was not carried out given that it is not suitable for ACSM instruments, as recently learnt from an intercomparison of 13 Q-ACSM instruments (Fröhlich et al., 2015).

Eliminado: Figure S5



### 3.2 Time series and average composition of submicron aerosol. Seasonal variation

The average concentration (P25, P75) of the ACSM components plus BC concentrations during the study period was  $7.3 \mu\text{g m}^{-3}$  (3.1, 10.2). The highest concentrations were measured during the warm periods (average  $10.3 \mu\text{g m}^{-3}$ ), defined as the periods with most of the days with average  $T > 20^\circ\text{C}$  (from 14<sup>th</sup> June to 9<sup>th</sup> October 2012 and from 13<sup>th</sup> June to 9<sup>th</sup> July 2013). The lowest concentrations were recorded during the cold period (average  $5.8 \mu\text{g m}^{-3}$ ), which includes a period with most of the days with average  $T < 13^\circ\text{C}$  (from 28<sup>th</sup> October 2012 to 7<sup>th</sup> April 2013) (Figure 3). The average monthly concentrations, following the described variation, can be seen in Figure 4. This is in agreement with the seasonal variations observed during a long time period (2002-2010) by Cusack et al. (2012). The summer increase is associated with the recirculation of air masses that prevent air renovation, the low precipitation (Figure S2), and the formation of secondary aerosols enhanced by the maximum solar radiation (Figure S2). The lower winter concentrations can be explained by the high frequency of Atlantic advections (Figure S1) and the higher precipitation rates, although occasional high concentrations are attributed to winter anticyclonic scenarios (Pey et al., 2010). The seasonal variation of  $\text{PM}_{10}$  concentrations at MSY is also influenced by the evolution of the boundary layer height, which is lower during wintertime and increases during summertime, especially during the central hours of the day. Changes in the origin of air masses also determined the seasonal variation of  $\text{PM}_{10}$  concentrations.

On average, the most abundant component was OA ( $3.8 \mu\text{g m}^{-3}$ ), followed, in this order, by sulphate ( $1.3 \mu\text{g m}^{-3}$ ), ammonium ( $0.8 \mu\text{g m}^{-3}$ ), nitrate ( $0.8 \mu\text{g m}^{-3}$ ), BC ( $0.4 \mu\text{g m}^{-3}$ ) and chloride ( $< 0.1 \mu\text{g m}^{-3}$ ). The OA contribution varied throughout the year, reaching 60% of the total  $\text{PM}_{10}$  in the summer period (June, July and August) and decreasing progressively down to 43% in February (Figure 4). The contribution of sulphate followed the same seasonal variation, from about 20% in the warmer months to about 8% in the colder months. The nitrate contribution showed an inverse trend, with higher relative contributions in the winter and much lower in summer. These seasonal variations were already observed in previous studies using off-line filter sampling (Pey et al., 2009; Ripoll et al., 2014b) and can be attributed to a higher SOA contribution, favoured formation of sulphate, and nitrate gas/aerosol partitioning leading to vaporization of ammonium nitrate during the warmer period.

When investigating the diurnal patterns, it is observed that OA, nitrate and BC concentrations reach the maximum at around 14h UTC in summer, whereas sulphate and ammonium show a delayed increase in their concentrations, peaking at around 16h UTC (Figure 5). The reasons for this shift may obey to the different origin of each component.

Eliminado: Figure 3

Eliminado: Figure 4

Código de campo cambiado

Eliminado: Figure S2

Eliminado: Figure S2

Eliminado: Figure S1

Eliminado: Figure 4

Eliminado: Figure 5

Whereas the OA, nitrate and BC are transported with the breeze from the populated areas and the valley towards the regional background site, the sulphate can also be transported from further away, i.e. from over the Mediterranean Sea due to shipping emissions. Later in the day, when the breeze is developed in the opposite direction (from inland towards the coast), the concentrations of OA, BC and nitrate decrease, whereas the sulphate and ammonium concentrations remained high for longer time (until about 19h UTC). This is due to the more regional character of ammonium sulphate, which is present in a wider area due to its longer lifetime in the atmosphere (Seinfeld and Pandis, 2006) and hence remains longer at MSY. In addition to the transport of pollutants, local SOA can be formed (see section 3.5 for discussion). Specific episodes may differ from this average behaviour owing to specific atmospheric characteristics, for which sulphate concentrations increase simultaneously with OA, but the most common variation is the one described here. On the other hand, in winter, all the components show an increase at around 15h UTC, and concentrations remain high until around 22h UTC, when they start to decrease to reach a minimum around 9h UTC (Figure 5). This simultaneous variation indicates that the pollutants are transported from the nearby polluted areas to MSY with the breeze.

Eliminado: Figure 5

### 3.3 Influence of the type of scenario on submicron aerosol

The total PM<sub>1</sub> concentrations were investigated as a function of the type of scenario, finding the lowest concentrations during Mediterranean episodes and Atlantic advections, and the highest during North African outbreaks, European episodes and Winter Anticyclonic episodes (Figure 6). Some differences in the relative chemical composition as a function of the type of scenario were found (Figure 6). OA and sulphate relative contributions were higher under regional and North African episodes. This may be due to the higher formation of secondary aerosols enhanced by the higher temperature and solar radiation during these episodes. See additional discussion about formation of SOA in section 3.5. Moreover, the higher sulphate concentrations under regional episodes may also be due to the enhanced regional mixing, as shown by the flatter diurnal pattern shown for this pollutant (Figure S6). Sulphate relative contribution was also high when Mediterranean air masses affected MSY probably owing to the impact of shipping emissions. On the other hand, nitrate relative contribution was found to be higher for Winter Anticyclonic and European episodes. For both cases the colder weather compared to the rest of the year is partly responsible for the higher nitrate concentrations. During Winter Anticyclonic episodes, the stagnant conditions favouring the accumulation of polluted air masses that are transported from the Barcelona metropolitan

Eliminado: Figure 6

Eliminado: Figure 6

Eliminado: Figure S6

area towards MSY may also be responsible for the high nitrate concentrations (Pey et al., 2010). Note that this transport takes place later in the day than in warm conditions, thus reaching the maximum concentrations between 15h UTC and 22h UTC, and that the day-night difference is much higher than for other scenarios (Figure S6). During European episodes, the higher nitrate concentration can be attributed to the long range transport of nitrate from Europe to the study area, although this type of episodes often take place under anticyclonic conditions and hence the nitrate may have a local origin at lower heights, whereas European nitrate is transported at higher altitudes, as it was seen by Ripoll et al. (2014b).

The relative chemical composition as a function of the total concentration was also investigated, but no clear patterns were identified, meaning that there is not a prevalent component for low or for high concentrations (Figure S7).

### 3.4 Wildfire episode

A wildfire episode took place from 22 to 26 July 2012 (Figure 7) at 100 km to the NE of MSY, affecting a wide area (Figure S8). It resulted in an average ACSM components + BC concentrations of  $16.5 \mu\text{g m}^{-3}$  over the five-days period. Mainly, the components whose concentrations increased significantly were OA, nitrate and BC, reaching 30-min values of  $50 \mu\text{g m}^{-3}$ ,  $4.5 \mu\text{g m}^{-3}$  and  $3.6 \mu\text{g m}^{-3}$ , respectively, which are 9, 8 and 7 times higher than their respective summer averages. The average relative concentration during this episode was dominated by OA (73%).

In order to investigate the wildfire source, an unconstrained source apportionment (PMF) of the organic aerosol fraction during this episode was carried out. The PMF resulted in two factors, one representing the fresh biomass burning organic aerosol (named as BBOA\_MSY) and another one interpreted as the mix of other OA sources and aged BBOA, named as OOAm (where the m stands for mix). The interpretation of the factors is based on their mass spectral source profiles and the time series of their contributions. The BBOA\_MSY shows higher peaks for the specific tracers of biomass burning ( $m/z$  60 and  $m/z$  73) (Alfarra et al., 2007) than the OOAm, which indicates that the primary BBOA is well represented by this factor. Moreover, the f44 (ratio of  $m/z$  44 (mostly  $\text{CO}_2^+$ ) to total signal in the component mass spectra), an indicator of oxygenated organic species (Alfarra et al., 2007), was higher for the OOAm than for the BBOA\_MSY factor, which indicates that this factor corresponds to a more oxidized aerosol. On the other hand, the f43 is higher than the f44 in the BBOA\_MSY factor, whereas it is the other way around (f44 much higher than f43) in the OOAm. These differences in relative intensities indicate the differences in the age of the aerosol (Ng et al., 2010) and

Eliminado: Figure S6

Código de campo cambiado

Eliminado: Figure S7

Eliminado: Figure 7

Eliminado: Figure S8

further lead to differentiate the factors as fresh BBOA and OOAm. The SOA formation from biomass burning has been reported to be quick (Heringa et al., 2011), and hence part of the OOAm factor is formed of aged BBOA, which also explains that the time series of the OOAm factor partially tracks that of the BBOA\_MSY. The BBOA\_MSY profile found here is very similar to a BBOA profile found for Montseny in March 2009 (Minguillón et al., 2011) (<https://sites.google.com/site/amsglobaldatabase>) and to an average profile for BBOA from various datasets (Ng et al., 2011a) (Figure S9). The f60 in the BBOA\_MSY factor is 0.014, similar to the f60 in these other two BBOA profiles (0.017 and 0.024). It has been also compared to the BBOA found in the background of Paris (Crippa et al., 2013), with which some more differences were found, mainly our profile has higher  $m/z$  43 and  $m/z$  41 signals and lower  $m/z$  60 (Figure S9). This BBOA\_MSY mass spectrum is considered specific for the study area and hence it can be later used for other studies in the region, to be fed to the ME-2 model in order to quantify the BBOA contribution. We have done so in the present study for the winter period. Whereas the time series of both factors were similar, the BBOA\_MSY contribution showed more intense peaks, and the increase in the OOAm was slightly higher for the second part of the main peak on the 23 July.

Eliminado: Figure S9

Eliminado: Figure S9

### 3.5 Source apportionment of organic aerosol

The source apportionment of organic aerosol was carried out separately for the warmer period (14 June to 9 October 2012) and the colder period (28 October 2012 to 7 April 2013). The days of the wildfire event were excluded from the warmer period dataset. The separation in two seasons was done to better characterize the source profiles of the different sources, especially the different types of OOA, given that it is expected to vary throughout the year.

The application of ME-2 to the warmer period resulted in a solution with 3 factors: a hydrocarbon-like OA (HOA), a semi-volatile oxygenated OA (SV-OOA) and a low-volatile oxygenated OA (LV-OOA). This solution was chosen based on several tests with different number of factors and different  $\alpha$ -values for the constrained factors, taking into account the correlations with external data, the diurnal patterns and the residuals, following the strategy described by Crippa et al. (2014) and Canonaco et al. (2013). The HOA factor was constrained using an average HOA factor (HOA\_avg) from different datasets (Ng et al., 2011a). An  $\alpha$ -value range from 0.05 to 0.3 was explored and an  $\alpha$ -value of 0.2 was finally selected, which was a compromise between a higher squared Pearson correlation coefficient between HOA and BC (which increased when increasing the  $\alpha$ -value) and the physically meaningful profiles of the

Código de campo cambiado

Código de campo cambiado

whole solution (i.e. assessing the profiles of the LV-OOA and SV-OOA factors). Hence, the  $\alpha$ -value 0.05 did not reach converge, and the  $\alpha$ -value 0.1 resulted in not-well-resolved OOA factors. BC concentrations correlated moderately with HOA of the chosen solution (squared Pearson coefficient  $R^2 = 0.51$ , [Table S1](#)). The SV-OOA shows higher 43-to-44 ratio compared to the LV-OOA, together with a lower  $f_{44}$ , which are the main differences between these two profiles ([Figure 8a](#)). The BBOA contribution in summer is expected to be low based on previous studies carried out in July 2009 (Minguillón et al., 2011) and on the low  $f_{60}$  registered in the present study in summer ([Figure S10](#)), which is below the background threshold (0.003) established by Cubison et al. (2011). Hence, the BBOA factor was not identified and it was not constrained by the ME-2 in summer. The correlations of the two OOA factors with external secondary pollutants is not very high (LV-OOA with ammonium shows  $R^2 = 0.43$ , LV-OOA with sulphate shows  $R^2 = 0.34$ , and SV-OOA with nitrate shows  $R^2 = 0.16$ , [Table S1](#)). Nevertheless, the source profiles are well defined. The 4-factors solution was investigated and resulted in a split of the LV-OOA factor. The residuals of the 3-factors solution showed an increase between 12h and 15h (which did not disappear in the 4-factors solution), hence indicating the difficulty in explaining the variation of the OA during the middle hours of the day. This pattern was also observed for the  $m/z$  43 variable residuals, whereas it was not observed for other variables. Therefore, the difficulty in the OA explanation may be more related to the SOA formation processes rather than to primary OA sources. [Further details on the chosen solution can be found in the supplementary material \(Figures S11 to S15\).](#)

During the warmer period, the HOA accounted for 13% ( $0.7 \mu\text{g m}^{-3}$ ), whereas the LV-OOA and the SV-OOA accounted for 44% and 41% of the total OA ( $2.5 \mu\text{g m}^{-3}$  and  $2.3 \mu\text{g m}^{-3}$ ), respectively, hence remaining 2% of unexplained OA mass ([Figure 8c](#)). The time series is shown in [Figure S16](#). As explained before, the location and meteorological conditions at MSY result in an increase of pollutants concentrations starting at mid-morning, caused by the breeze transport from populated areas to the regional site. This variation is clearly observed for BC ([Figure 9](#)), which showed a moderate correlation with HOA ( $R^2 = 0.51$ ). Nevertheless, the midday increase in the concentration of SV-OOA is larger than that of BC, and therefore it cannot be only explained by the transport of pollutants, including the SOA formed during the transport, but it is attributed to the formation of SOA during these hours in MSY. Hence, the SOA formation can be estimated as the additional increase with respect to that of BC (considered in % of the average concentration during the night hours), which results in a local SOA formation of  $1.1 \mu\text{g m}^{-3}$ . This SOA may result mainly from biogenic precursors, in agreement with the 70% of non-fossil SOA found in March 2009 (Minguillón et al., 2011). The flatter diurnal pattern of LV-OOA ([Figure 9](#)) points to a more regional and well-oxidized

Eliminado: Figure 8

Eliminado: Figure S10

Código de campo cambiado

Eliminado: 17

Eliminado: 2

Eliminado: 2

Eliminado: 39

Eliminado: 4

Eliminado: 2

Eliminado: 7

Eliminado: Figure 8

Eliminado: Figure S11

Eliminado: Figure 9

Eliminado: Figure 9

aerosol, which could be interpreted as the regional background SOA. The difference in the diurnal patterns between LV-OOA and SV-OOA is more evident during the regional episodes, evidencing the mixing of the background pollutants (LV-OOA) and the formation of SOA on site (part of the SV-OOA) (Figure S17). This SOA formation during warm periods was also observed by Cusack et al. (2013), who studied nucleation and particle growth events, identifying both of them even under polluted conditions at MSY.

Eliminado: Figure S12

In the colder period, the application of ME-2 resulted in a solution with 3 factors:

hydrocarbon-like OA (HOA), biomass burning OA (BBOA) and oxygenated OA (OOA) (Figure 8b). A solution with two OOA factors was investigated and it was not meaningfully

Eliminado: Figure 8

interpretable. Probably the small temperature range variation in winter results in not enough diurnal variation in f43 and f44 for a split of the OOA in SV-OOA and LV-OOA. As per the warmer period, the final solution was chosen based on the strategy described by Crippa et al.

(2014) and Canonaco et al. (2013). For coherence with the warmer period, the HOA factor was

Código de campo cambiado

based in an average HOA factor (HOA\_avg) from different datasets (Ng et al., 2011a), and it

Código de campo cambiado

was constrained with an a-value of 0.1. This a-value was chosen based on the correlation

between the HOA contribution and the BC concentrations found for different a-values tests,

the source profiles obtained for the rest of the sources (i.e. assuring that they were

meaningful), and a preference for relatively low a-values to avoid mixing of OOA sources into

the HOA source. The HOA contribution of the chosen solution shows a relatively strong

correlation with BC concentrations (squared Pearson coefficient  $R^2=0.70$ , Table S1). The HOA

spectral profiles found for summer and winter are quite similar, and hence the HOA

contributions in summer and winter can be compared directly. The BBOA factor was decided

to be constrained based on the f60 signal, which was above the aforementioned threshold of

0.003 (Figure S10). It was based in the BBOA\_MSJ profile found for the wildfire episode that

Eliminado: Figure S10

took place during this study, constrained with an a-value of 0.1. The a-value was chosen with

the following criteria: preference for a low a-value given that the anchor profile used was site-

specific, residuals for the  $m/z$  60 not showing any diurnal pattern, contribution of the BBOA

factor to the total  $m/z$  60 (which reached 64% for the chosen solution). The resulting BBOA

profile has a higher  $m/z$  44 signal than the BBOA\_MSJ, which may indicate differences in the

biomass burning emissions from the wildfire event compared to the emissions from regular

biomass burning, or it could indicate that the BBOA contribution identified here may be

partially mixed with some oxidized OA. The single winter OOA factor identified shows higher

f44 than both LV-OOA and SV-OOA in summer. This higher degree of oxidation of the OA in

winter indicates that there is less newly-formed SOA during winter compared to summer. A

similar variation was observed in Zurich (Canonaco et al., 2014). The OOA contribution

correlates moderately with sulphate ( $R^2=0.49$ ), relatively strongly with nitrate ( $R^2=0.73$ ) and more strongly with ammonium ( $R^2=0.79$ , Table S1). Further details on the chosen solution can be found in the supplementary material (Figures S11 to S15).

The major OA constituent in winter was the OOA, with 59% ( $1.5 \mu\text{g m}^{-3}$ ), whereas the HOA and BBOA accounted for 12% ( $0.3 \mu\text{g m}^{-3}$ ) and 28% ( $0.7 \mu\text{g m}^{-3}$ ) of the total OA, respectively, with only 1% of the OA mass remaining unexplained (Figure 8d). Note that the BBOA contribution may be mixed with some OOA as stated before, given the relatively high signal at  $m/z$  44 and hence the pure BBOA contribution would be lower than that determined. Actually it accounts for 6% of the total signal at  $m/z$  44. Nevertheless, strong correlation ( $R^2=0.77$ ) was found between the BBOA contribution and the potassium concentrations determined in 24-h  $\text{PM}_{10}$  samples (Figure S18), which further confirms the existence of this source at MSY in winter. The relative BBOA contributions found in the present study are similar to those found in a previous study in March 2009 using a HR-ToF-AMS, where the HOA represented 7% of the total OA, the BBOA contributed with 9% and the rest was attributed to OOA (Minguillón et al., 2011; Crippa et al., 2014). The discrepancy in the BBOA contribution (29% vs 9%) may be due to the different sampling periods (the current study included Nov 2012-March 2013 whereas the previous study only included March 2009), to the mixture of some OOA in the BBOA factor for the present study, and/or to the possible increase of biomass burning due to the climate and energy policies in the last five years.

The average daily pattern shown by the different OA sources in winter (Figure 9) resembles that of BC, nitrate, sulphate and ammonium (Figure 5), with an increase of pollutants concentrations starting at around 10h UTC and reaching high concentrations at around 13h UTC. No significant differences in the daily pattern were observed for different meteorological episodes, other than the different concentrations (Figure S17). This daily increase is attributed to the transport from populated areas to the mountain site with the breeze. This variation is observed for all the components and therefore the local formation of SOA is deduced to be low in winter.

#### 4 CONCLUSIONS

The deployment of an ACSM at the regional background site of Montseny during one year allowed for the characterization of  $\text{PM}_{10}$  composition and its variation as a function of time of the year and atmospheric scenarios. The OA sources were also identified and studied.

Strong correlation ( $R^2=0.66$ ) was found between total mass determined by ACSM components + BC and  $\text{PM}_{10}$  determined by an optical particle counter with a slope near to

Eliminado: Figure 8

Eliminado: Figure S13

Eliminado: Figure 9

Eliminado: Figure 5

Eliminado: Figure S12

unity. The suitability of the application of a composition-dependent collection efficiency (CE) was confirmed.

Strong correlations were found between the ACSM measurements and off-line measurements (filters) for sulphate ( $R^2=0.93$ ), ammonium ( $R^2=0.68$ ) and nitrate ( $R^2=0.82$ ). Nevertheless the slopes differ more than 20% from the unity for nitrate and ammonium.

The comparison of the OA measured by the ACSM with the OC measured in filter samples points to a current underestimation of the RIE established for OA.

A wildfire episode affected significantly the organic aerosol concentrations. The source profile of fresh BBOA for this specific episode was characterized and it resembles those from other studies. [The BBOA contribution in winter correlates with the PM<sub>1</sub> potassium concentrations.](#)

OA was the major component of submicron aerosol on average and especially during the warm periods. Three organic sources were identified by PMF in summer: HOA, SV-OOA and LV-OOA; and three sources in winter: HOA, BBOA and OOA. SOA was the major constituent of the OA at MSY, being more than 80% of total OA in summer and about 60% in winter. The in-situ formation of SOA in summer, happening around midday, was estimated to be  $1.1 \mu\text{g m}^{-3}$  on average (20% of OA).

Sulphate concentrations were higher in summer, while nitrate concentrations were higher in winter due to environmental conditions (temperature, relative humidity and solar radiation, among others). Sulphate originates from a wider area and is affected by the shipping emissions from the Mediterranean, while the rest of the components may have a nearer origin.

As typical for mountain sites, all the pollutants were affected by the general breeze regime, leading to an increase from mid-morning until the afternoon, and a decrease until the evening.

## ACKNOWLEDGEMENTS

This study was supported by the Spanish Ministry of Economy and Competitiveness and FEDER funds under the project PRISMA (CGL2012-39623-C02-1), by the Generalitat de Catalunya (AGAUR ~~2014~~ SGR33 and the DGQA), and by the European Union Seventh Framework Programme (FP7/ 2007-2013) through ACTRIS (grant agreement no 262254). M.C. Minguillón was partially funded by the JAE-Doc CSIC program, co-funded by the European Social Fund (ESF). A. Ripoll was partially funded by a PhD grant from the Spanish Ministry of Economy and Competitiveness through CARIATI (CGL2008-06294/CLI) project.

Eliminado: 2015



## FIGURE CAPTIONS

Figure 1. ACSM components + BC concentrations vs  $PM_{10}$  measured by the optical counter coloured by the sampling time (dd/mm/yyyy). Line and parameters correspond to least orthogonal distance fit ( $y=a+bx$ ). The wild fire period is excluded from the fit.

Figure 2. ACSM components concentrations vs 24-h samples concentrations. Lines and parameters correspond to least orthogonal distance fits.

Figure 3. Time series of ACSM components and BC concentrations during the whole study period.

Figure 4. Monthly relative chemical composition of submicron aerosol. The numbers on top of each bar represent the average monthly concentration. n is the number of data points for each month (right axis).

Figure 5. Average daily pattern for (a) the warmer and (b) the colder periods. Note that OA is plotted in the right axis.

Figure 6. Relative chemical composition of submicron aerosol as a function of the type of scenario. The numbers on top of each bar represent the average concentration for each type of scenario. n is the number of data points for each type of scenario (right axis).

Figure 7. (a) Time series of ACSM components and BC concentrations and pie chart of the average chemical composition during the wildfire episode from 22<sup>nd</sup> to 26<sup>th</sup> July 2012. (b) Time series of the contribution of the BBOA\_MSY and Aged BBOA sources identified by PMF. (c) Source profile of the BBOA\_MSY and Aged BBOA sources.

Figure 8. Mass spectral profiles of the organic sources identified for (a) summer and (b) winter. Average contribution of the organic sources to total OA for (c) summer and (d) winter. The white fraction of the pie charts corresponds to unexplained mass.

Figure 9. Average daily patterns of the organic sources contributions and BC concentrations for (a) summer and (b) winter. Error bars represent standard deviations.

## SUPPLEMENTARY MATERIAL

Figure S1. Frequency of type of scenario for each of the months of the study period.

Figure S2. Temperature, relative humidity, wind direction and speed, solar radiation and precipitation hourly data at MSY during the study period.

Figure S3. Time-dependent CE calculated with the Middlebrook approach (Middlebrook et al., 2012).

Figure S4. ACSM components + BC concentrations vs mass concentration calculated from Scanning Mobility Particle Sizer (SMPS) data coloured by the sampling time (dd/mm/yyyy). Data availability for SMPS data covered only 2012 period. Line and parameters correspond to least orthogonal distance fit ( $y=a+bx$ ). The wild fire period is excluded from the fit.

Figure S5. Schematic comparison of ACSM components + BC concentrations vs  $PM_{10}$  concentrations from OPC corrected with gravimetric determinations. The numbers indicate the slopes found for experimental data for Montseny during June 2012 to July 2013. The 2.25 corresponds to the slope of OA (ACSM) vs OM estimated from OC (filters) as  $2*OC$ .

Figure S6. Average daily pattern for (a) Atlantic advections (ATL), (b) North African episodes (NAF), (c) regional episodes (REG), and (d) Winter Anticyclonic episodes (WAE). Note that OA is plotted in the right axis.

Figure S7. Relative chemical composition as a function of average concentration and number of data points for each range of concentrations. No clear differences are observed.

674 Figure S8. Total optical depth, sulphate surface concentration, dust surface concentration, and smoke  
675 surface concentration from the NAAPS model for 23, 24 and 25 July 2012 (wildfire event) (a-c), and  
676 satellite images from 22 and 23 July 2012 from The Earth Observing System Data and Information  
677 System (EOSDIS), NASA's Earth Science Data Systems Program (d, e).

Eliminado: f

678 Figure S9. Comparison of the BBOA factor found for the wildfire episode (BBOA\_MSY) with other  
679 BBOA profiles found in the literature (Ng et al., 2011a; Crippa et al., 2014).

680 Figure S10. Time series of f60 (unitless) and OA concentration ( $\mu\text{g m}^{-3}$ ) throughout the study period at  
681 MSY. Dashed line corresponds to the 0.5% threshold for the f60 determined by Cubison et al. (2011).

Código de campo cambiado

682 Figure S11. Q/Qexp vs number of factors for the warmer and the colder periods. The grey dot in the  
683 colder period corresponds to a solution with an a-value of 0.2 for the BBOA factor, given that there  
684 was no convergence with an a-value of 0.1 for the 2-factors solution.

685 Figure S12. Weighted residuals vs m/z for the warmer and the colder periods.

686 Figure S13. Time series of the measured and reconstructed OA concentrations for the warmer and the  
687 colder periods.

688 Figure S14. Time series of Q/Qexp for the warmer and the colder periods.

689 Figure S15. Q/Qexp vs m/z for the warmer and the colder periods.

690 Figure S16. Time series of the OA sources in the warmer (top) and the colder (bottom) periods.

Eliminado: 11

691 Figure S17. Average daily pattern for Atlantic advections (ATL), for the warmer and the colder periods,  
692 regional episodes (REG) (only warmer period), and Winter Anticyclonic episodes (WAE) (only colder  
693 period).

Eliminado: 12

694 Figure S18. Contribution of BBOA in winter (averaged to 24-h periods matching the filter sampling) vs  
695 potassium concentrations in  $\text{PM}_{10}$ .

Eliminado: 13

696 Table S1. Squared Pearson correlation coefficients between OA sources/types and BC, sulphate,  
697 nitrate and ammonium for the warmer and the colder periods

698

699

## 700 REFERENCES

701 Aiken, A. C., Decarlo, P. F., Kroll, J. H., Worsnop, D. R., Huffman, J. A., Docherty, K. S.,  
702 Ulbrich, I. M., Mohr, C., Kimmel, J. R., Sueper, D., Sun, Y., Zhang, Q., Trimborn, A., Northway,  
703 M., Ziemann, P. J., Canagaratna, M. R., Onasch, T. B., Alfarra, M. R., Prevot, A. S. H., Dommen,  
704 J., Duplissy, J., Metzger, A., Baltensperger, U., and Jimenez, J. L.: O/C and OM/OC ratios of  
705 primary, secondary, and ambient organic aerosols with high-resolution time-of-flight aerosol  
706 mass spectrometry, Environ. Sci. Technol., 42, 4478-4485, 2008.

707 Alastuey, A., Minguillón, M. C., Pérez, N., Querol, X., Viana, M., and de Leeuw, F.: PM10  
708 measurement methods and correction factors: 2009 status report, ETC/ACM Technical Paper  
709 2011/21, 2011.

710 Alfarra, M. R., Prevot, A. S. H., Szidat, S., Sandradewi, J., Weimer, S., Lanz, V. A.,  
711 Schreiber, D., Mohr, M., and Baltensperger, U.: Identification of the mass spectral signature of  
712 organic aerosols from wood burning emissions, Environ. Sci. Technol., 41, 5770-5777, 2007.

713 Alves, C., Vicente, A., Pio, C., Kiss, G., Hoffer, A., Decesari, S., Prevôt, A. S. H.,  
714 Minguillón, M. C., Querol, X., Hillamo, R., Spindler, G., and Swietlicki, E.: Organic compounds in

719 aerosols from selected European sites - Biogenic versus anthropogenic sources, *Atmos.*  
720 *Environ.*, 59, 243-255, 2012.

721 Bougiatioti, A., Stavroulas, I., Kostenidou, E., Zampas, P., Theodosi, C., Kouvarakis, G.,  
722 Canonaco, F., Prévôt, A. S. H., Nenes, A., Pandis, S. N., and Mihalopoulos, N.: Processing of  
723 biomass-burning aerosol in the eastern Mediterranean during summertime, *Atmos. Chem.*  
724 *Phys.*, 14, 4793-4807, 2014.

725 Budisulistiorini, S. H., Canagaratna, M. R., Croteau, P. L., Marth, W. J., Baumann, K.,  
726 Edgerton, E. S., Shaw, S. L., Knipping, E. M., Worsnop, D. R., Jayne, J. T., Gold, A., and Surratt, J.  
727 D.: Real-time continuous characterization of secondary organic aerosol derived from isoprene  
728 epoxydiols in downtown Atlanta, Georgia, using the aerodyne aerosol chemical speciation  
729 monitor, *Environ. Sci. Technol.*, 47, 5686-5694, 2013.

730 Budisulistiorini, S. H., Canagaratna, M. R., Croteau, P. L., Baumann, K., Edgerton, E. S.,  
731 Kollman, M. S., Ng, N. L., Verma, V., Shaw, S. L., Knipping, E. M., Worsnop, D. R., Jayne, J. T.,  
732 Weber, R. J., and Surratt, J. D.: Intercomparison of an Aerosol Chemical Speciation Monitor  
733 (ACSM) with ambient fine aerosol measurements in downtown Atlanta, Georgia, *Atmos. Meas.*  
734 *Tech.*, 7, 1929-1941, 10.5194/amt-7-1929-2014, 2014.

735 Canagaratna, M. R., Jayne, J. T., Jimenez, J. L., Allan, J. D., Alfarra, M. R., Zhang, Q.,  
736 Onasch, T. B., Drewnick, F., Coe, H., Middlebrook, A., Delia, A., Williams, L. R., Trimborn, A. M.,  
737 Northway, M. J., DeCarlo, P. F., Kolb, C. E., Davidovits, P., and Worsnop, D. R.: Chemical and  
738 microphysical characterization of ambient aerosols with the aerodyne aerosol mass  
739 spectrometer, *Mass Spectrom. Rev.*, 26, 185-222, 2007.

740 Canonaco, F., Crippa, M., Slowik, J. G., Baltensperger, U., and Prévôt, A. S. H.: SoFi, an  
741 IGOR-based interface for the efficient use of the generalized multilinear engine (ME-2) for the  
742 source apportionment: ME-2 application to aerosol mass spectrometer data, *Atmospheric*  
743 *Measurement Techniques*, 6, 3649-3661, 2013.

744 Canonaco, F., Slowik, J. G., Baltensperger, U., and Prévôt, A. S. H.: Inverse relationship  
745 between the degree of oxidation of OOA (oxygenated organic aerosol) and the oxidant OX (O<sub>3</sub>  
746 +NO<sub>2</sub>) due to biogenic emissions, *Atmos. Chem. Phys. Discuss.*, 14, 28079-28104,  
747 10.5194/acpd-14-28079-2014, 2014.

748 Carbone, S., Saarikoski, S., Frey, A., Reyes, F., Reyes, P., Castillo, M., Gramsch, E., Oyola,  
749 P., Jayne, J., Worsnop, D., and Hillamo, R.: Chemical characterization of submicron Aerosol  
750 particles in Santiago de Chile, *Aerosol and Air Quality Research*, 13, 462-473, 2013.

751 Cavalli, F., Viana, M., Yttri, K. E., Genberg, J., and Putaud, J. P.: Toward a standardised  
752 thermal-optical protocol for measuring atmospheric organic and elemental carbon: the  
753 EUSAAR protocol, *Atmos. Meas. Tech.*, 3, 79-89, 10.5194/amt-3-79-2010, 2010.

754 Crippa, M., DeCarlo, P. F., Slowik, J. G., Mohr, C., Heringa, M. F., Chirico, R., Poulain, L.,  
755 Freutel, F., Sciare, J., Cozic, J., Di Marco, C. F., Elsasser, M., Nicolas, J. B., Marchand, N., Abidi,  
756 E., Wiedensohler, A., Drewnick, F., Schneider, J., Borrmann, S., Nemitz, E., Zimmermann, R.,  
757 Jaffrezo, J. L., Prévôt, A. S. H., and Baltensperger, U.: Wintertime aerosol chemical composition  
758 and source apportionment of the organic fraction in the metropolitan area of Paris, *Atmos.*  
759 *Chem. Phys.*, 13, 961-981, 10.5194/acp-13-961-2013, 2013.

760 Crippa, M., Canonaco, F., Lanz, V. A., Äijälä, M., Allan, J. D., Carbone, S., Capes, G.,  
761 Ceburnis, D., Dall'Osto, M., Day, D. A., DeCarlo, P. F., Ehn, M., Eriksson, A., Freney, E., Ruiz, L.

762 H., Hillamo, R., Jimenez, J. L., Junninen, H., Kiendler-Scharr, A., Kortelainen, A. M., Kulmala, M.,  
763 Laaksonen, A., Mensah, A. A., Mohr, C., Nemitz, E., O'Dowd, C., Ovadnevaite, J., Pandis, S. N.,  
764 Petäjä, T., Poulain, L., Saarikoski, S., Sellegri, K., Swietlicki, E., Tiitta, P., Worsnop, D. R.,  
765 Baltensperger, U., and Prévôt, A. S. H.: Organic aerosol components derived from 25 AMS data  
766 sets across Europe using a consistent ME-2 based source apportionment approach, *Atmos.*  
767 *Chem. Phys.*, 14, 6159-6176, 2014.

768 Cubison, M. J., Ortega, A. M., Hayes, P. L., Farmer, D. K., Day, D., Lechner, M. J., Brune,  
769 W. H., Apel, E., Diskin, G. S., Fisher, J. A., Fuelberg, H. E., Hecobian, A., Knapp, D. J., Mikoviny,  
770 T., Riemer, D., Sachse, G. W., Sessions, W., Weber, R. J., Weinheimer, A. J., Wisthaler, A., and  
771 Jimenez, J. L.: Effects of aging on organic aerosol from open biomass burning smoke in aircraft  
772 and laboratory studies, *Atmos. Chem. Phys.*, 11, 12049-12064, 2011.

773 Cusack, M., Alastuey, A., Pérez, N., Pey, J., and Querol, X.: Trends of particulate matter  
774 (PM<sub>2.5</sub>) and chemical composition at a regional background site in the Western  
775 Mediterranean over the last nine years (2002–2010), *Atmos. Chem. Phys.*, 12, 8341-8357,  
776 10.5194/acp-12-8341-2012, 2012.

777 Cusack, M., Pérez, N., Pey, J., Wiedensohler, A., Alastuey, A., and Querol, X.: Variability  
778 of sub-micrometer particle number size distributions and concentrations in the Western  
779 Mediterranean regional background, *Tellus, Series B: Chemical and Physical Meteorology*, 65,  
780 2013.

781 Fröhlich, R., Crenn, V., Setyan, A., Belis, C. A., Canonaco, F., Favez, O., Riffault, V.,  
782 Slowik, J. G., Aas, W., Aijälä, M., Alastuey, A., Artiñano, B., Bonnaire, N., Bozzetti, C., Bressi, M.,  
783 Carbone, C., Coz, E., Croteau, P. L., Cubison, M. J., Esser-Gietl, J. K., Green, D. C., Gros, V.,  
784 Heikkinen, L., Herrmann, H., Jayne, J. T., Lunder, C. R., Minguillón, M. C., Močnik, G., O'Dowd,  
785 C. D., Ovadnevaite, J., Petralia, E., Poulain, L., Priestman, M., Ripoll, A., Sarda-Estève, R.,  
786 Wiedensohler, A., Baltensperger, U., Sciare, J., and Prévôt, A. S. H.: ACTRIS ACSM  
787 intercomparison – Part 2: Intercomparison of ME-2 organic source apportionment results from  
788 15 individual, co-located aerosol mass spectrometers, *Atmos. Meas. Tech. Discuss.*, 8, 1559-  
789 1613, 10.5194/amtd-8-1559-2015, 2015.

790 Hawkins, L. N., Russell, L. M., Covert, D. S., Quinn, P. K., and Bates, T. S.: Carboxylic  
791 acids, sulfates, and organosulfates in processed continental organic aerosol over the southeast  
792 Pacific Ocean during VOCALS-REx 2008, *Journal of Geophysical Research: Atmospheres*, 115,  
793 10.1029/2009jd013276, 2010.

794 Heringa, M. F., DeCarlo, P. F., Chirico, R., Tritscher, T., Dommen, J., Weingartner, E.,  
795 Richter, R., Wehrle, G., Prévôt, A. S. H., and Baltensperger, U.: Investigations of primary and  
796 secondary particulate matter of different wood combustion appliances with a high-resolution  
797 time-of-flight aerosol mass spectrometer, *Atmos. Chem. Phys.*, 11, 5945-5957, 2011.

798 IPCC: Climate Change 2013: The Physical Science Basis. Contribution of Working Group  
799 I to the Fifth Assessment Report of the Intergovernmental Panel on Climate Change, edited by:  
800 Stocker, T. F., Qin, D., Plattner, G.-K., Tignor, M., Allen, S. K., Boschung, J., Nauels, A., Xia, Y.,  
801 Bex, V., and Midgley, P. M., Cambridge University Press, Cambridge, United Kingdom and New  
802 York, NY, USA, 1535 pp pp., 2013.

803 Jimenez, J. L., Canagaratna, M. R., Donahue, N. M., Prevot, A. S. H., Zhang, Q., Kroll, J.  
804 H., DeCarlo, P. F., Allan, J. D., Coe, H., Ng, N. L., Aiken, A. C., Docherty, K. S., Ulbrich, I. M.,  
805 Grieshop, A. P., Robinson, A. L., Duplissy, J., Smith, J. D., Wilson, K. R., Lanz, V. A., Hueglin, C.,

806 Sun, Y. L., Tian, J., Laaksonen, A., Raatikainen, T., Rautiainen, J., Vaattovaara, P., Ehn, M.,  
807 Kulmala, M., Tomlinson, J. M., Collins, D. R., Cubison, M. J., Dunlea, E. J., Huffman, J. A.,  
808 Onasch, T. B., Alfarra, M. R., Williams, P. I., Bower, K., Kondo, Y., Schneider, J., Drewnick, F.,  
809 Borrmann, S., Weimer, S., Demerjian, K., Salcedo, D., Cottrell, L., Griffin, R., Takami, A.,  
810 Miyoshi, T., Hatakeyama, S., Shimono, A., Sun, J. Y., Zhang, Y. M., Dzepina, K., Kimmel, J. R.,  
811 Sueper, D., Jayne, J. T., Herndon, S. C., Trimborn, A. M., Williams, L. R., Wood, E. C.,  
812 Middlebrook, A. M., Kolb, C. E., Baltensperger, U., and Worsnop, D. R.: Evolution of organic  
813 aerosols in the atmosphere, *Science*, 326, 1525-1529, 2009.

814 Liu, P. S. K., Deng, R., Smith, K. A., Williams, L. R., Jayne, J. T., Canagaratna, M. R.,  
815 Moore, K., Onasch, T. B., Worsnop, D. R., and Deshler, T.: Transmission efficiency of an  
816 aerodynamic focusing lens system: Comparison of model calculations and laboratory  
817 measurements for the aerodyne aerosol mass spectrometer, *Aerosol Sci. Technol.*, 41, 721-  
818 733, 2007.

819 Middlebrook, A. M., Bahreini, R., Jimenez, J. L., and Canagaratna, M. R.: Evaluation of  
820 composition-dependent collection efficiencies for the Aerodyne aerosol mass spectrometer  
821 using field data, *Aerosol Sci. Technol.*, 46, 258-271, 2012.

822 Millán, M. M., Salvador, R., Mantilla, E., and Kallos, G.: Photooxidant dynamics in the  
823 Mediterranean basin in summer: Results from European research projects, *Journal of*  
824 *Geophysical Research D: Atmospheres*, 102, 8811-8823, 1997.

825 Minguillón, M. C., Perron, N., Querol, X., Szidat, S., Fahrni, S. M., Alastuey, A., Jimenez,  
826 J. L., Mohr, C., Ortega, A. M., Day, D. A., Lanz, V. A., Wacker, L., Reche, C., Cusack, M., Amato,  
827 F., Kiss, G., Hoffer, A., Decesari, S., Moretti, F., Hillamo, R., Teinilä, K., Seco, R., Peñuelas, J.,  
828 Metzger, A., Schallhart, S., Müller, M., Hansel, A., Burkhardt, J. F., Baltensperger, U., and Prévôt,  
829 A. S. H.: Fossil versus contemporary sources of fine elemental and organic carbonaceous  
830 particulate matter during the DAURE campaign in Northeast Spain, *Atmos. Chem. Phys.*, 11,  
831 12067-12084, 10.5194/acp-11-12067-2011, 2011.

832 Ng, N. L., Canagaratna, M. R., Zhang, Q., Jimenez, J. L., Tian, J., Ulbrich, I. M., Kroll, J. H.,  
833 Docherty, K. S., Chhabra, P. S., Bahreini, R., Murphy, S. M., Seinfeld, J. H., Hildebrandt, L.,  
834 Donahue, N. M., DeCarlo, P. F., Lanz, V. A., Prévôt, A. S. H., Dinar, E., Rudich, Y., and Worsnop,  
835 D. R.: Organic aerosol components observed in Northern Hemispheric datasets from Aerosol  
836 Mass Spectrometry, *Atmos. Chem. Phys.*, 10, 4625-4641, 10.5194/acp-10-4625-2010, 2010.

837 Ng, N. L., Canagaratna, M. R., Jimenez, J. L., Zhang, Q., Ulbrich, I. M., and Worsnop, D.  
838 R.: Real-time methods for estimating organic component mass concentrations from aerosol  
839 mass spectrometer data, *Environ. Sci. Technol.*, 45, 910-916, 2011a.

840 Ng, N. L., Herndon, S. C., Trimborn, A., Canagaratna, M. R., Croteau, P. L., Onasch, T. B.,  
841 Sueper, D., Worsnop, D. R., Zhang, Q., Sun, Y. L., and Jayne, J. T.: An Aerosol Chemical  
842 Speciation Monitor (ACSM) for routine monitoring of the composition and mass  
843 concentrations of ambient aerosol, *Aerosol Sci. Technol.*, 45, 770-784, 2011b.

844 Paatero, P., and Tapper, U.: Positive matrix factorization: a non-negative factor model  
845 with optimal utilization of error estimates of data values, *Environmetrics*, 5, 111-126, 1994.

846 Paatero, P.: The multilinear engine - a table-driven, least squares program for solving  
847 multilinear problems, including the n-way parallel factor analysis model, *Journal of*  
848 *Computational and Graphical Statistics*, 8, 854-888, 1999.

849 Pérez, N., Pey, J., Castillo, S., Viana, M., Alastuey, A., and Querol, X.: Interpretation of  
850 the variability of levels of regional background aerosols in the Western Mediterranean, *Sci.*  
851 *Total Environ.*, 407, 527-540, 2008.

852 Petit, J. E., Favez, O., Sciare, J., Crenn, V., Sarda-Estève, R., Bonnaire, N., Močnik, G.,  
853 Dupont, J. C., Haeffelin, M., and Leoz-Garziandia, E.: Two years of near real-time chemical  
854 composition of submicron aerosols in the region of Paris using an Aerosol Chemical Speciation  
855 Monitor (ACSm) and a multi-wavelength Aethalometer, *Atmos. Chem. Phys. Discuss.*, 14,  
856 24221-24271, 10.5194/acpd-14-24221-2014, 2014.

857 Petzold, A., Ogren, J. A., Fiebig, M., Laj, P., Li, S. M., Baltensperger, U., Holzer-Popp, T.,  
858 Kinne, S., Pappalardo, G., Sugimoto, N., Wehrli, C., Wiedensohler, A., and Zhang, X. Y.:  
859 Recommendations for reporting black carbon measurements, *Atmos. Chem. Phys.*, 13, 8365-  
860 8379, 2013.

861 Pey, J., Pérez, N., Castillo, S., Viana, M., Moreno, T., Pandolfi, M., López-Sebastián, J.  
862 M., Alastuey, A., and Querol, X.: Geochemistry of regional background aerosols in the Western  
863 Mediterranean, *Atmospheric Research*, 94, 422-435, 2009.

864 Pey, J., Pérez, N., Querol, X., Alastuey, A., Cusack, M., and Reche, C.: Intense winter  
865 atmospheric pollution episodes affecting the Western Mediterranean, *Sci. Total Environ.*, 408,  
866 1951-1959, 2010.

867 Pope III, C. A., and Dockery, D. W.: Health effects of fine particulate air pollution: Lines  
868 that connect, *Journal of the Air and Waste Management Association*, 56, 709-742, 2006.

869 Querol, X., Alastuey, A., Pey, J., Cusack, M., Pérez, N., Mihalopoulos, N., Theodosi, C.,  
870 Gerasopoulos, E., Kubilay, N., and Koçak, M.: Variability in regional background aerosols within  
871 the Mediterranean, *Atmos. Chem. Phys.*, 9, 4575-4591, 2009.

872 Querol, X., Alastuey, A., Viana, M., Moreno, T., Reche, C., Minguillón, M. C., Ripoll, A.,  
873 Pandolfi, M., Amato, F., Karanasiou, A., Pérez, N., Pey, J., Cusack, M., Vázquez, R., Plana, F.,  
874 Dall'Osto, M., De La Rosa, J., Sánchez De La Campa, A., Fernández-Camacho, R., Rodríguez, S.,  
875 Pio, C., Alados-Arboledas, L., Titos, G., Artíñano, B., Salvador, P., García Dos Santos, S., and  
876 Fernández Patier, R.: Variability of carbonaceous aerosols in remote, rural, urban and industrial  
877 environments in Spain: Implications for air quality policy, *Atmos. Chem. Phys.*, 13, 6185-6206,  
878 2013.

879 Querol, X., Alastuey, A., Pandolfi, M., Reche, C., Pérez, N., Minguillón, M. C., Moreno,  
880 T., Viana, M., Escudero, M., Orío, A., Pallarés, M., and Reina, F.: 2001-2012 trends on air quality  
881 in Spain, *Sci. Total Environ.*, 490, 957-969, 2014.

882 Ripoll, A., Minguillón, M. C., Pey, J., Jimenez, J. L., Day, D. A., Querol, X., and Alastuey,  
883 A.: Long-term real-time chemical characterization of submicron aerosols at Montsec (Southern  
884 Pyrenees, 1570 m a.s.l.), *Atmos. Chem. Phys. Discuss.*, 14, 28809-28844, 10.5194/acpd-14-  
885 28809-2014, 2014a.

886 Ripoll, A., Minguillón, M. C., Pey, J., Pérez, N., Querol, X., and Alastuey, A.: Joint  
887 analysis of continental and regional background environments in the Western Mediterranean:  
888 PM<sub>1</sub> and PM<sub>10</sub> concentrations and composition, *Atmos. Chem. Phys. Discuss.*, 14, 16001-  
889 16041, 10.5194/acpd-14-16001-2014, 2014b.

890 Shaw, S. L., Baumann, K., Budisulistiorini, S., Canagaratna, M., Croteau, P., Edgerton, E.,  
891 Jansen, J., Jayne, J., Knipping, E., Marth, W., Mueller, S., Ng, S., Surratt, J., Tanner, R., and  
892 Weber, R.: Operation of the aerosol chemical speciation monitor (ACSM) in the southeastern  
893 U.S, 2012, 110-114,

894 Sun, Y., Wang, Z., Dong, H., Yang, T., Li, J., Pan, X., Chen, P., and Jayne, J. T.:  
895 Characterization of summer organic and inorganic aerosols in Beijing, China with an Aerosol  
896 Chemical Speciation Monitor, *Atmos. Environ.*, 51, 250-259, 2012.

897 Sun, Y., Wang, Z., Fu, P., Jiang, Q., Yang, T., Li, J., and Ge, X.: The impact of relative  
898 humidity on aerosol composition and evolution processes during wintertime in Beijing, China,  
899 *Atmos. Environ.*, 77, 927-934, 2013a.

900 Sun, Y. L., Wang, Z. F., Fu, P. Q., Yang, T., Jiang, Q., Dong, H. B., Li, J., and Jia, J. J.:  
901 Aerosol composition, sources and processes during wintertime in Beijing, China, *Atmos. Chem.*  
902 *Phys.*, 13, 4577-4592, 2013b.

903 Takahama, S., Johnson, A., Guzman Morales, J., Russell, L. M., Duran, R., Rodriguez, G.,  
904 Zheng, J., Zhang, R., Toom-Saunty, D., and Leaitch, W. R.: Submicron organic aerosol in  
905 Tijuana, Mexico, from local and Southern California sources during the CalMex campaign,  
906 *Atmos. Environ.*, 70, 500-512, 2013.

907 Van Drooge, B. L., Cusack, M., Reche, C., Mohr, C., Alastuey, A., Querol, X., Prevot, A. S.  
908 H., Day, D. A., Jimenez, J. L., and Grimalt, J. O.: Molecular marker characterization of the  
909 organic composition of submicron aerosols from Mediterranean urban and rural environments  
910 under contrasting meteorological conditions, *Atmos. Environ.*, 61, 482-489, 2012.

911 Wiedensohler, A., Birmili, W., Nowak, A., Sonntag, A., Weinhold, K., Merkel, M.,  
912 Wehner, B., Tuch, T., Pfeifer, S., Fiebig, M., Fjåraa, A. M., Asmi, E., Sellegri, K., Depuy, R.,  
913 Venzac, H., Villani, P., Laj, P., Aalto, P., Ogren, J. A., Swietlicki, E., Williams, P., Roldin, P.,  
914 Quincey, P., Hüglin, C., Fierz-Schmidhauser, R., Gysel, M., Weingartner, E., Riccobono, F.,  
915 Santos, S., Gruning, C., Faloon, K., Beddows, D., Harrison, R., Monahan, C., Jennings, S. G.,  
916 O'Dowd, C. D., Marinoni, A., Horn, H. G., Keck, L., Jiang, J., Scheckman, J., McMurry, P. H.,  
917 Deng, Z., Zhao, C. S., Moerman, M., Henzing, B., De Leeuw, G., Löschau, G., and Bastian, S.:  
918 Mobility particle size spectrometers: Harmonization of technical standards and data structure  
919 to facilitate high quality long-term observations of atmospheric particle number size  
920 distributions, *Atmospheric Measurement Techniques*, 5, 657-685, 2012.

921

922

923

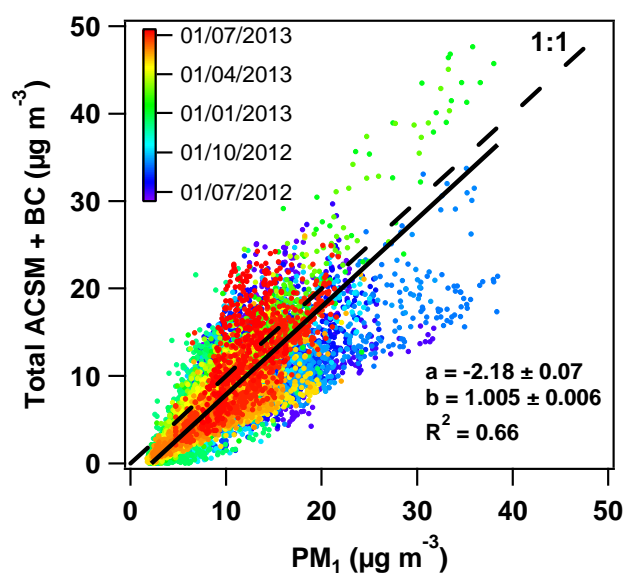


Figure 1

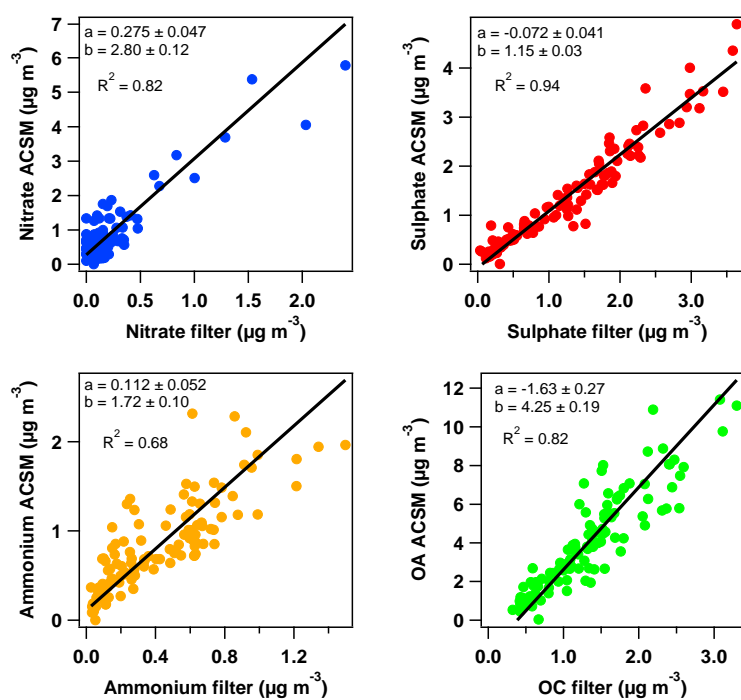


Figure 2



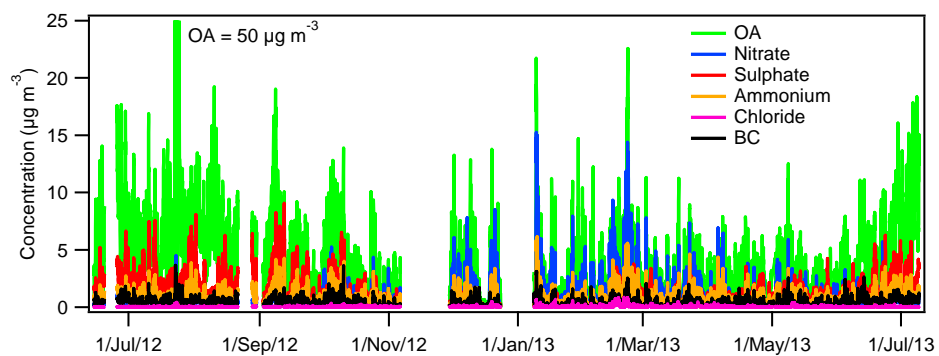


Figure 3

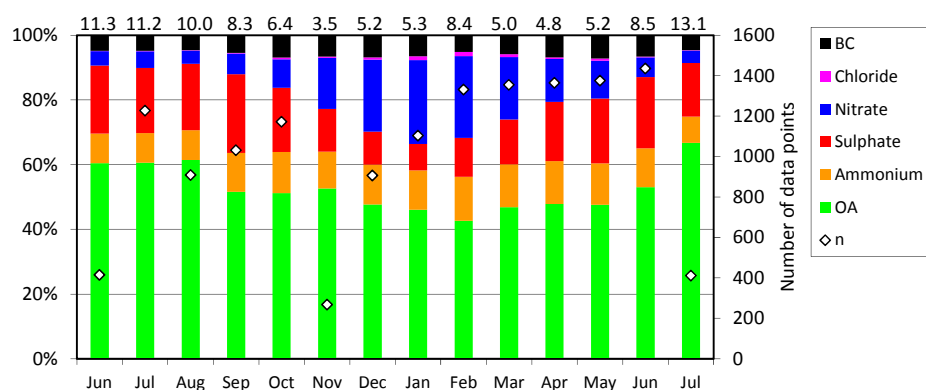
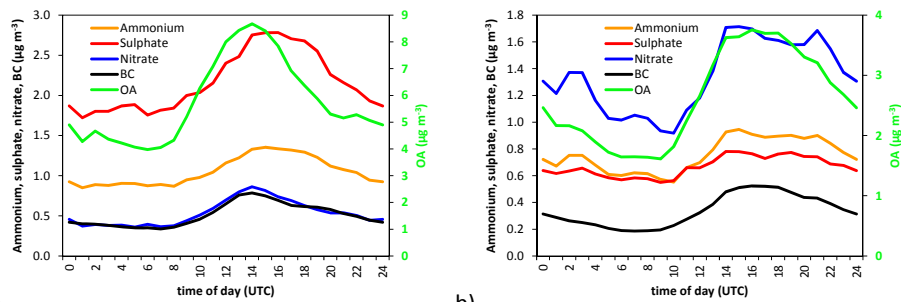


Figure 4



a)

b)

Figure 5

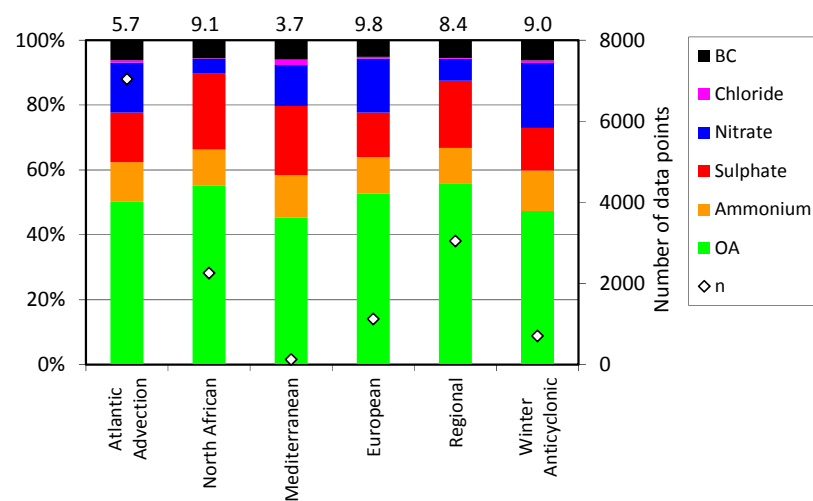
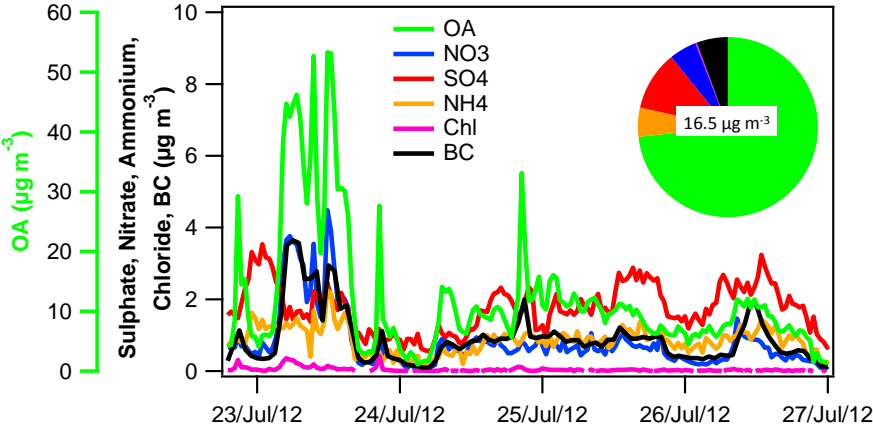
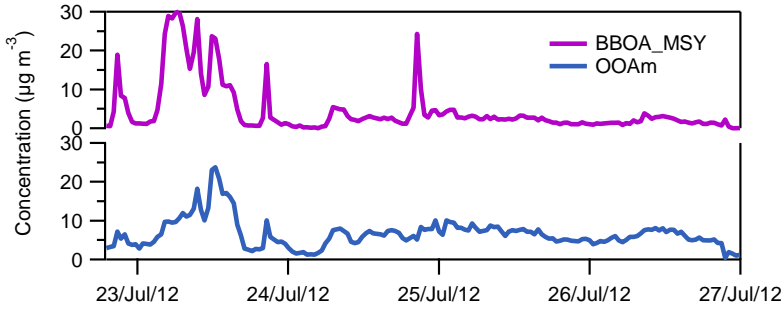


Figure 6

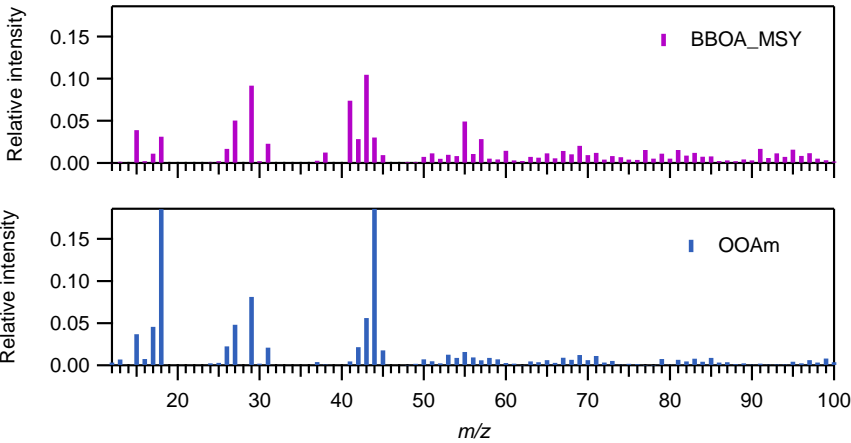
953



954 a)



955 b)



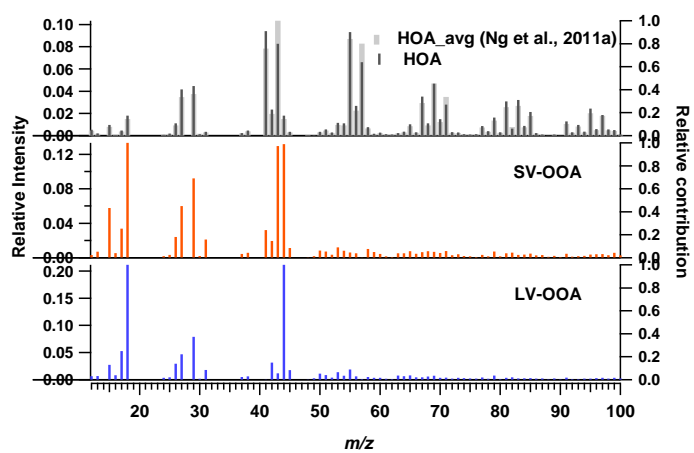
956

957 c)

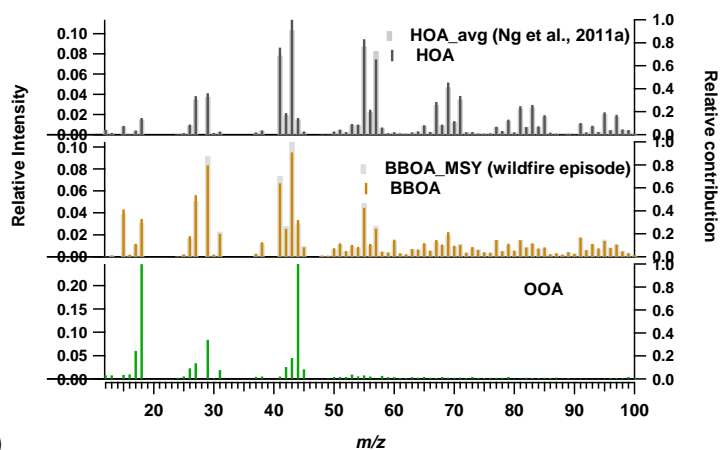
958 **Figure 7**

959

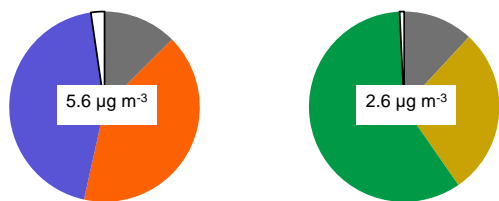
960



961 a)



962 b)



963 c) d)

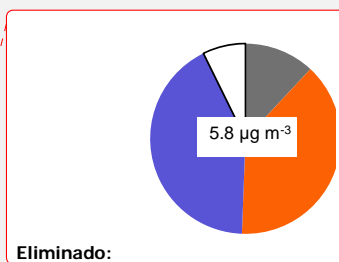


Figure 8

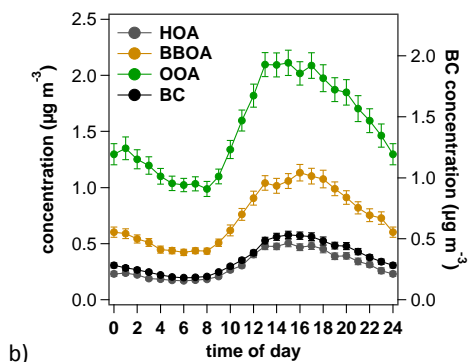
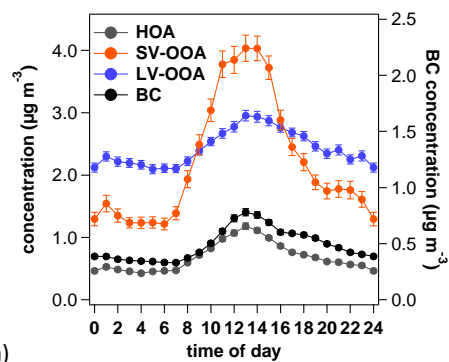


Figure 9

## **SUPPLEMENTARY MATERIAL**

### **Chemical characterization of submicron regional background aerosols in the Western Mediterranean using an Aerosol Chemical Speciation Monitor**

M.C. Minguillón<sup>1</sup>, A. Ripoll<sup>1,2</sup>, N. Pérez<sup>1</sup>, A.S.H. Prévôt<sup>3</sup>, F. Canonaco<sup>3</sup>, X. Querol<sup>1</sup>, A. Alastuey<sup>1</sup>

<sup>1</sup>Institute of Environmental Assessment and Water Research (IDAEA-CSIC), Jordi Girona 18-26, Barcelona, 08034, Spain

<sup>2</sup>Departament d'Astronomia i Meteorologia, Universitat de Barcelona, Martí i Franquès 1, 08028, Barcelona, Spain

<sup>3</sup>Paul Scherrer Institute, Laboratory of Atmospheric Chemistry, 5232 Villigen PSI, Switzerland

\*Corresponding author: mariacruz.minguillon@idaea.csic.es

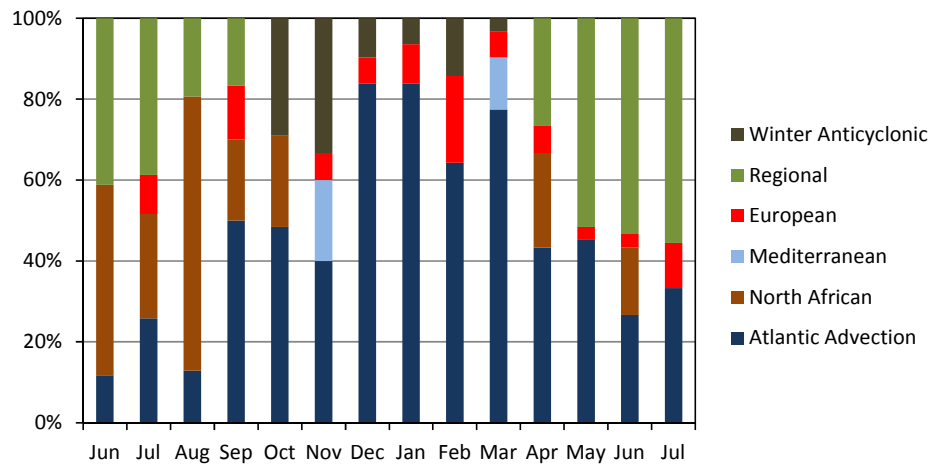


Figure S1. Frequency of type of scenario for each of the months of the study period.

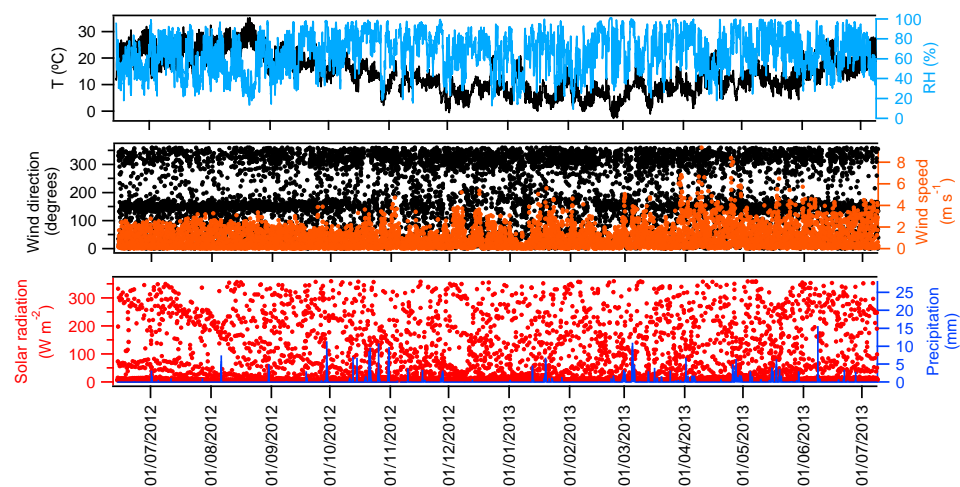


Figure S2. Hourly ambient temperature, relative humidity, wind direction and speed, solar radiation and precipitation at MSY during the study period. Date format dd/mm/yyyy.

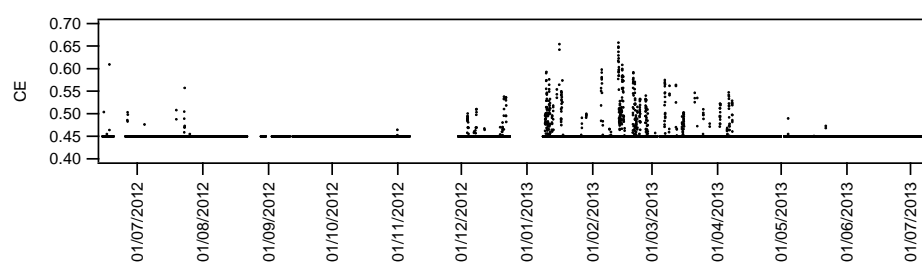


Figure S3. Time-dependent CE calculated with the Middlebrook approach (Middlebrook et al., 2012).

Date format dd/mm/yyyy.

Código de campo cambiado

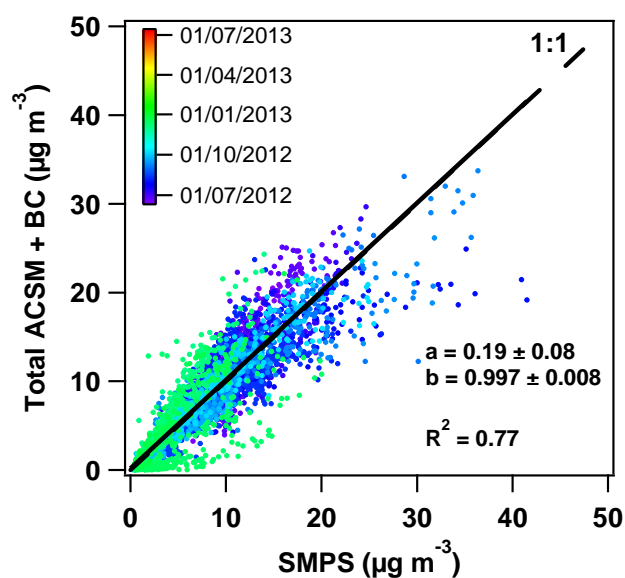


Figure S4. ACSM components + BC concentrations vs mass concentration calculated from Scanning Mobility Particle Sizer (SMPS) data coloured by the sampling time (dd/mm/yyyy). Data availability for SMPS data covered only 2012 period. Line and parameters correspond to least orthogonal distance fit ( $y=a+bx$ ). The wild fire period is excluded from the fit.

Eliminado: aaaa



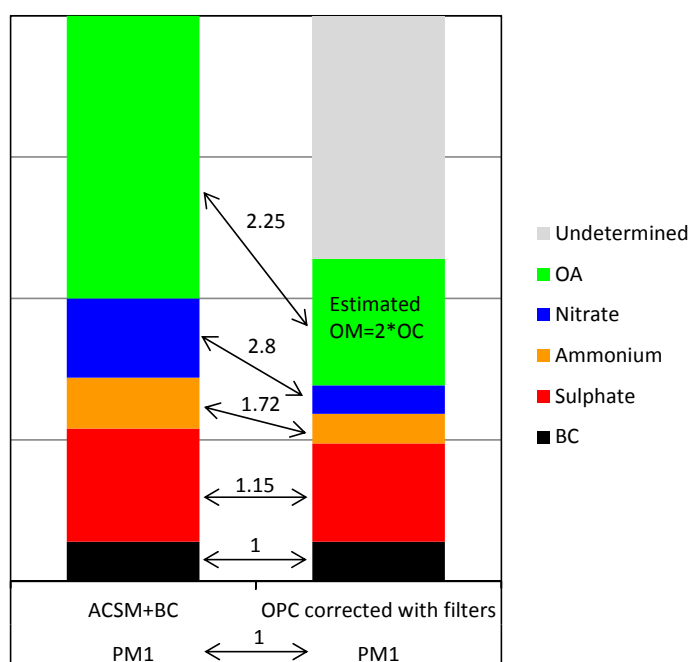


Figure S5. Schematic comparison of ACSM components + BC concentrations vs  $PM_1$  concentrations from OPC corrected with gravimetric determinations. The numbers indicate the slopes found for experimental data for Montseny during June 2012 to July 2013. The 2.25 corresponds to the slope of OA (ACSM) vs OM estimated from OC (filters) as  $2 \times OC$ .

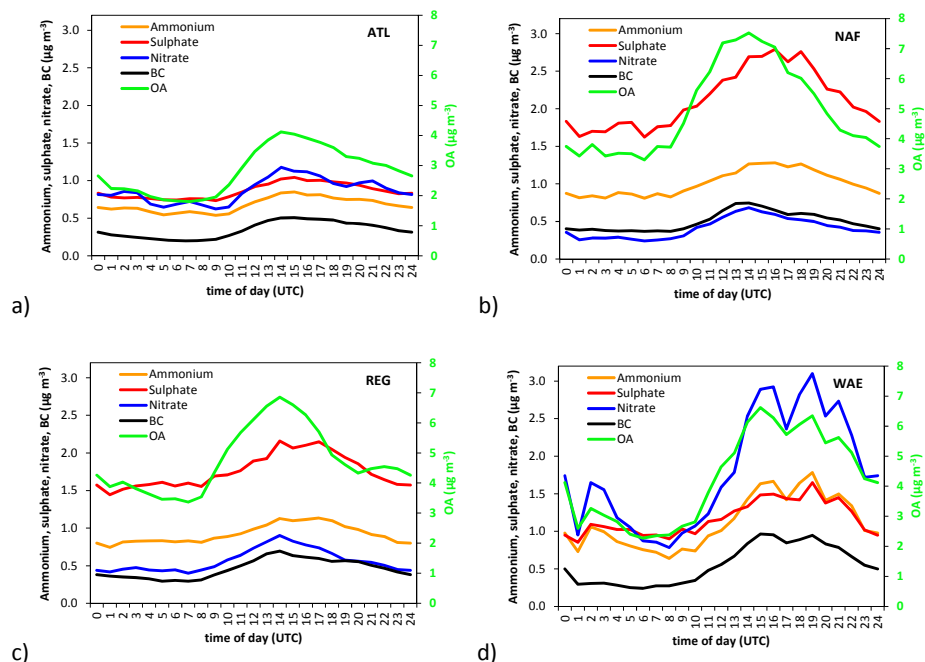


Figure S6. Average daily pattern for (a) Atlantic advections (ATL), (b) North African episodes (NAF), (c) regional episodes (REG), and (d) Winter Anticyclonic episodes (WAE). Note that OA is plotted in the right axis.

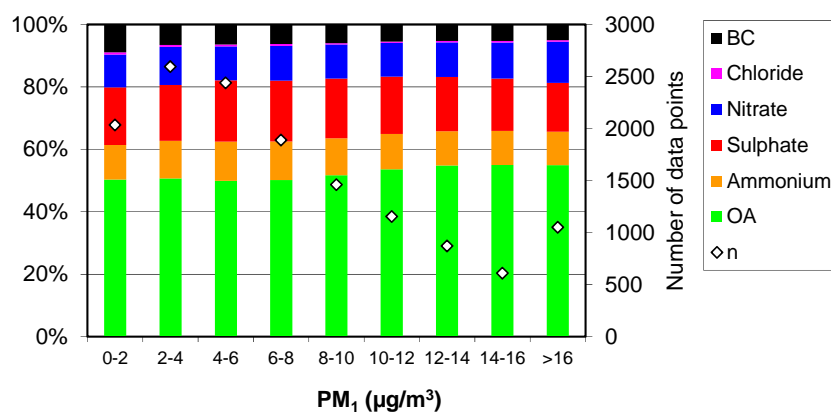
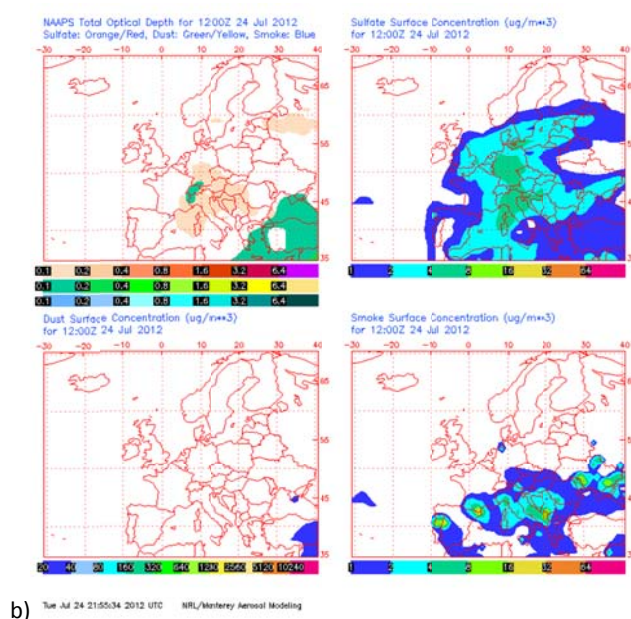
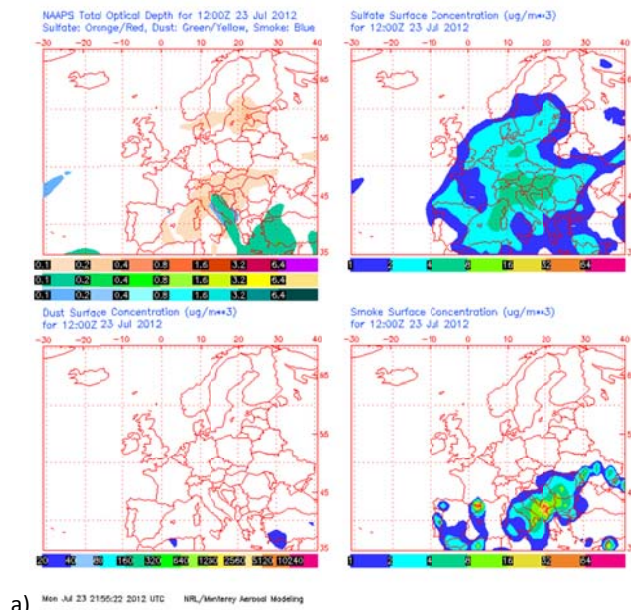


Figure S7. Relative chemical composition as a function of average concentration and number of data points for each range of concentrations. No clear differences are observed.



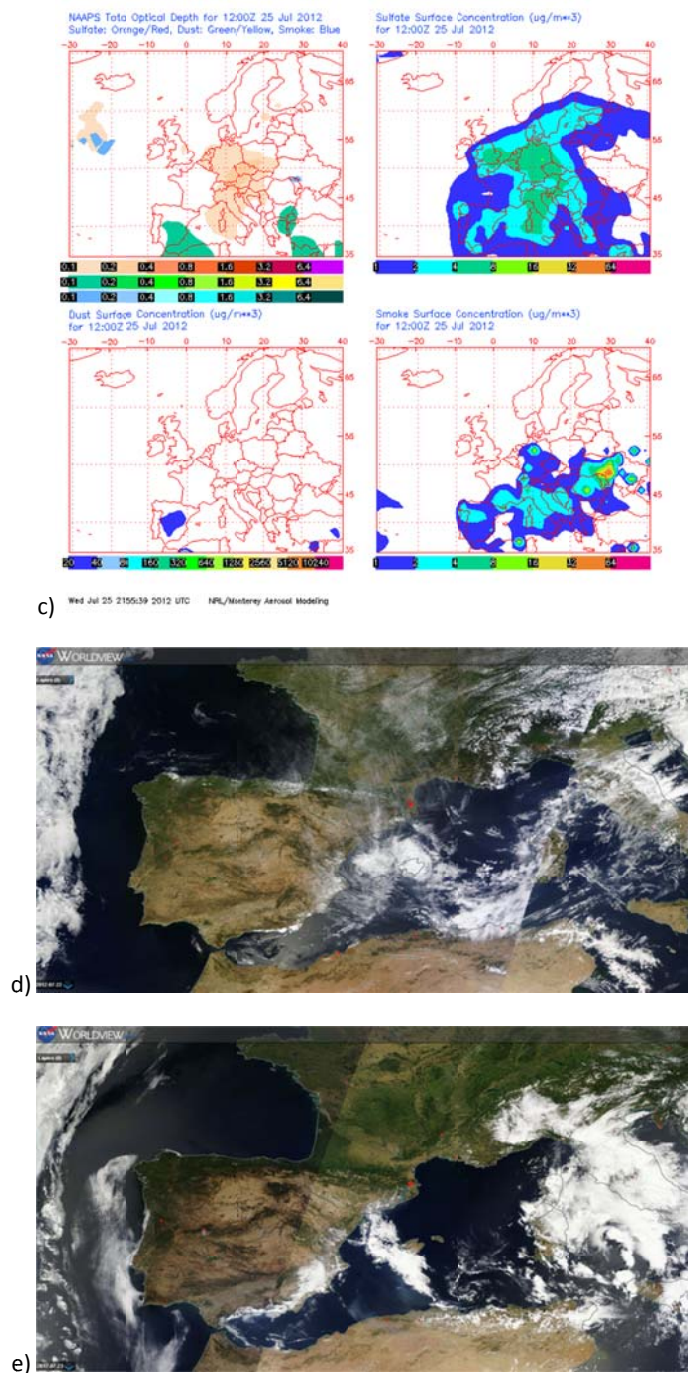
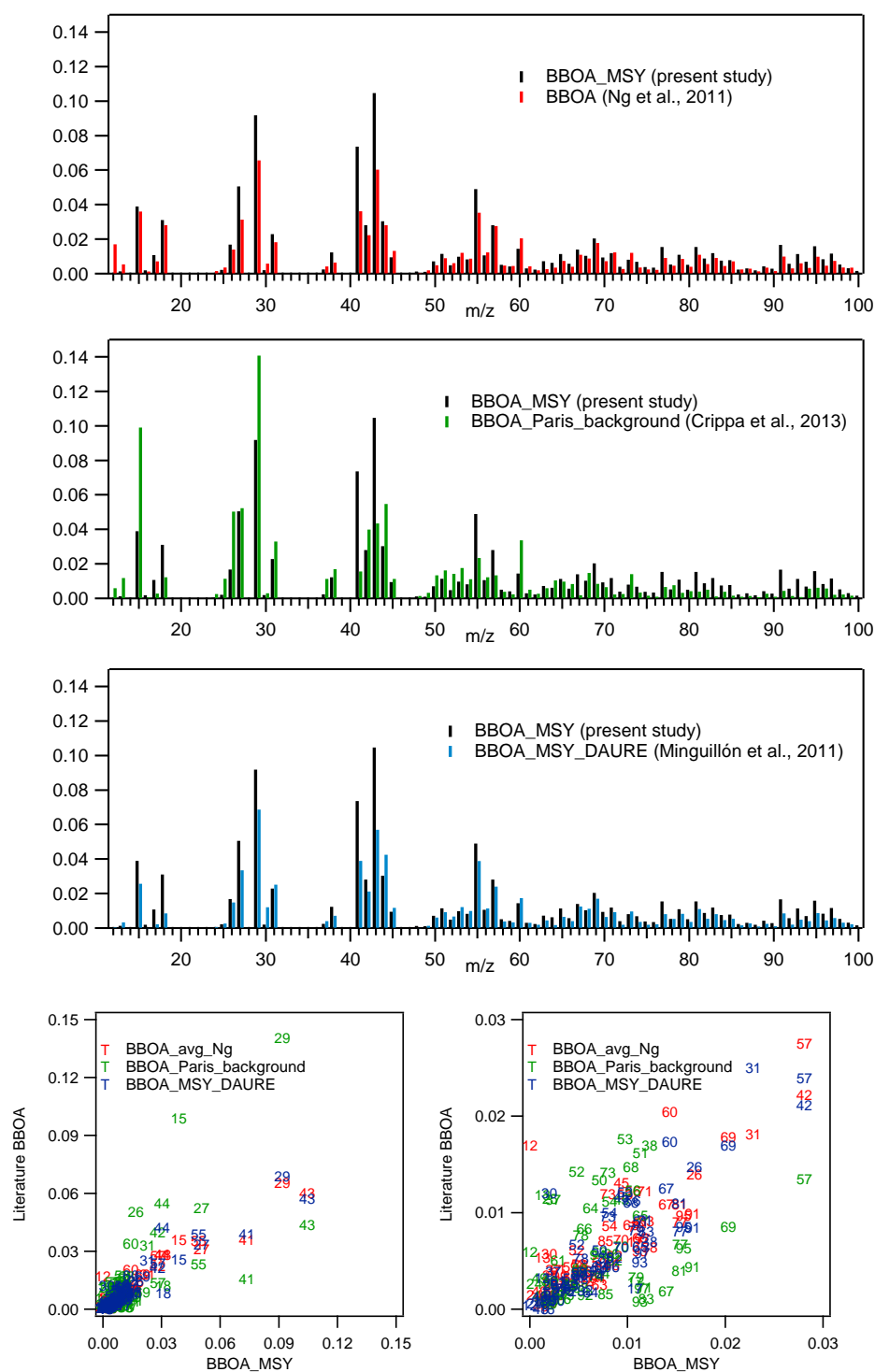


Figure S8. Total optical depth, sulphate surface concentration, dust surface concentration, and smoke surface concentration from the NAAPS model for 23, 24 and 25 July 2012 (wildfire event) (a-c), and satellite images from 22 and 23 July 2012 from The Earth Observing System Data and Information System (EOSDIS), NASA's Earth Science Data Systems Program (d, e).

Eliminado: f



**Figure S9. Comparison of the BBOA factor found for the wildfire episode (BBOA\_MSY) with other BBOA profiles found in the literature (Minguillón et al., 2011; Ng et al., 2011; Crippa et al., 2013). The scatter plot on the right is a zoom for values from 0.00 to 0.03.**

Código de campo cambiado

Código de campo cambiado

Código de campo cambiado

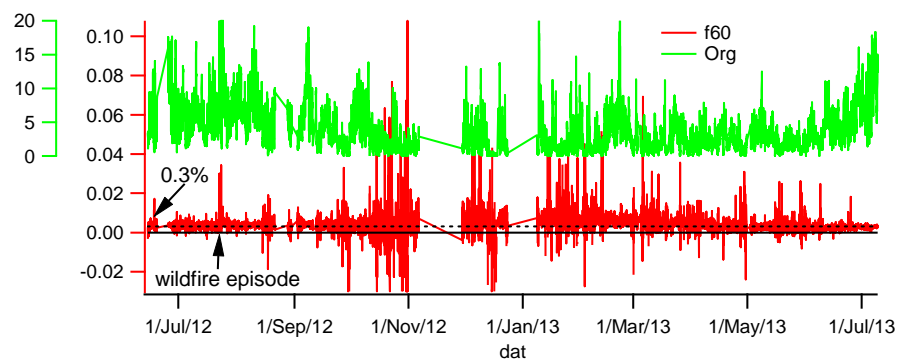


Figure S10. Time series of f60 (unitless) and OA concentration ( $\mu\text{g m}^{-3}$ ) throughout the study period at MSY. Dashed line corresponds to the 0.5% threshold for the f60 determined by Cubison et al. (2011).

Código de campo cambiado

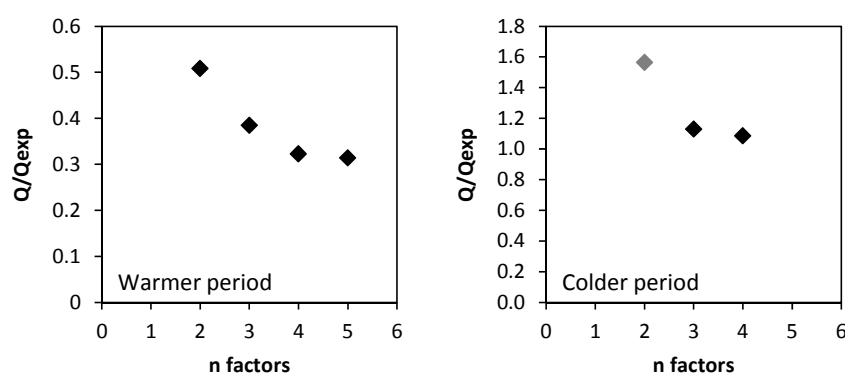
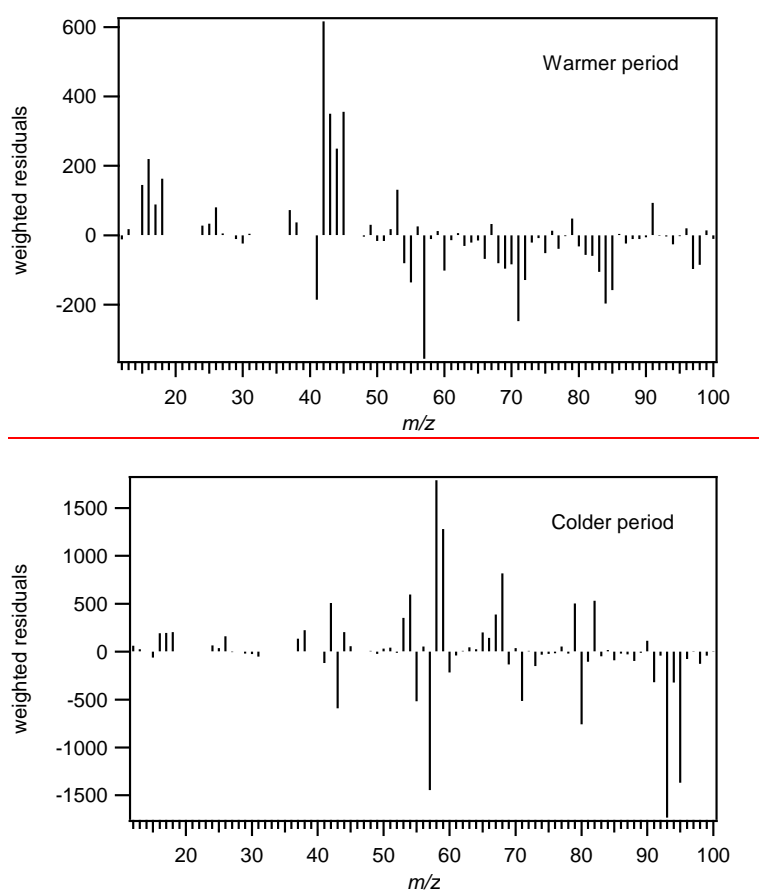
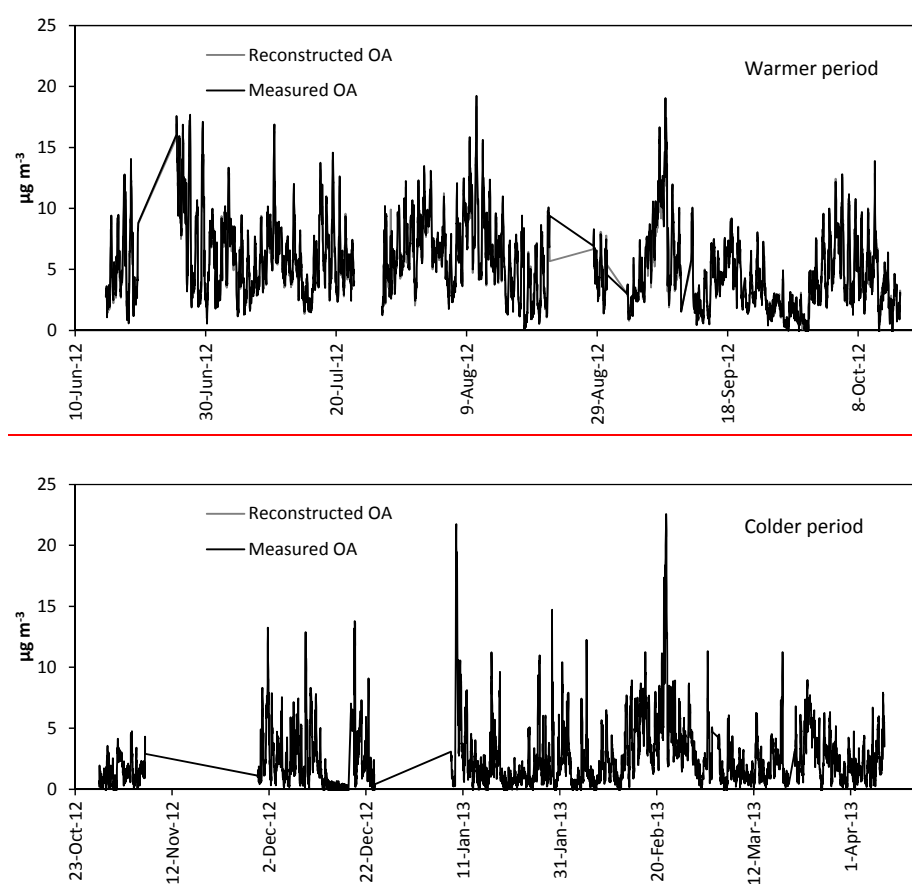


Figure S11.  $Q/Q_{\text{exp}}$  vs number of factors for the warmer and the colder periods. The grey dot in the colder period corresponds to a solution with an a-value of 0.2 for the BBOA factor, given that there was no convergence with an a-value of 0.1 for the 2-factors solution.



**Figure S12. Weighted residuals vs  $m/z$  for the warmer and the colder periods.**



**Figure S13. Time series of the measured and reconstructed OA concentrations for the warmer and the colder periods.**



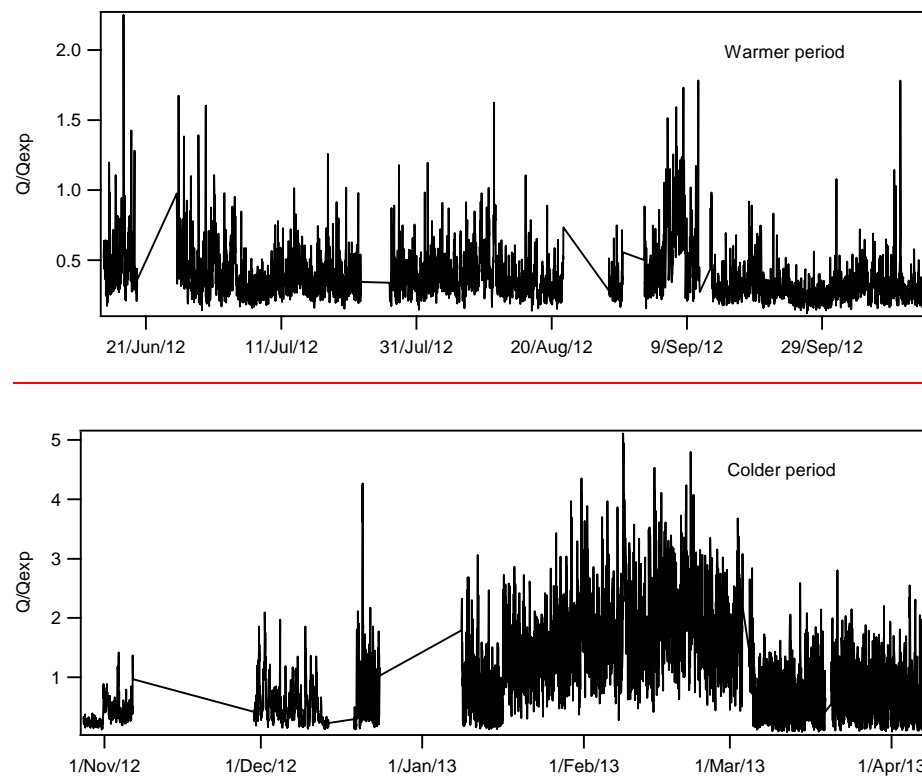


**Figure S14. Time series of  $Q/Q_{exp}$  for the warmer and the colder periods.**

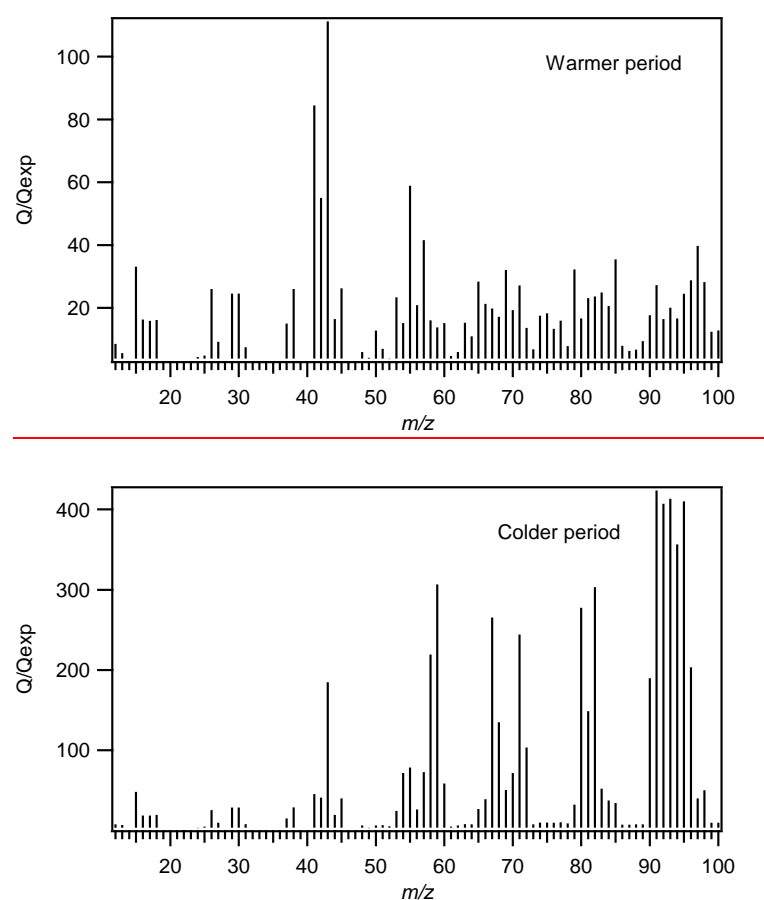


**Figure S15.  $Q/Q_{exp}$  vs  $m/z$  for the warmer and the colder periods.**

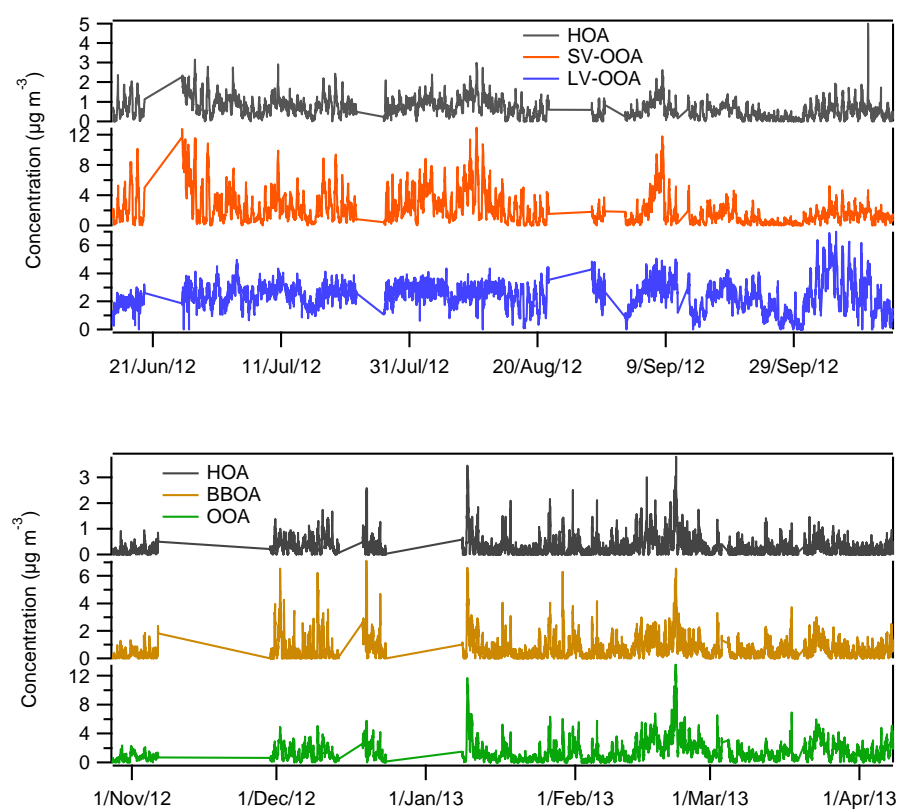


**Figure S16.** Time series of the OA sources in the warmer (top) and the colder (bottom) periods.

Eliminado: 11

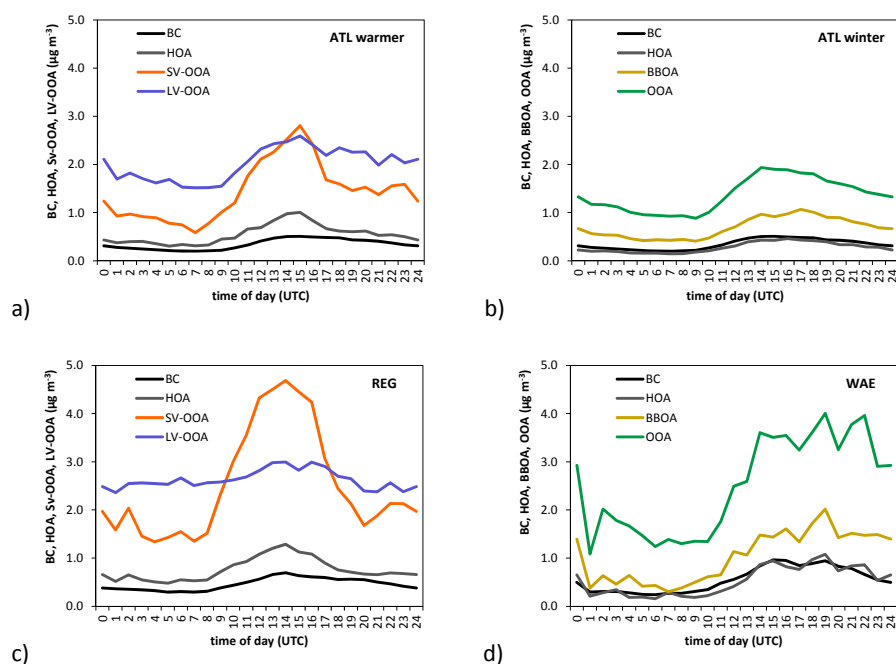


Figure S17. Average daily pattern for Atlantic advections (ATL), for the warmer and the colder periods, regional episodes (REG) (only warmer period), and Winter Anticyclonic episodes (WAE) (only colder period).

Eliminado: 12

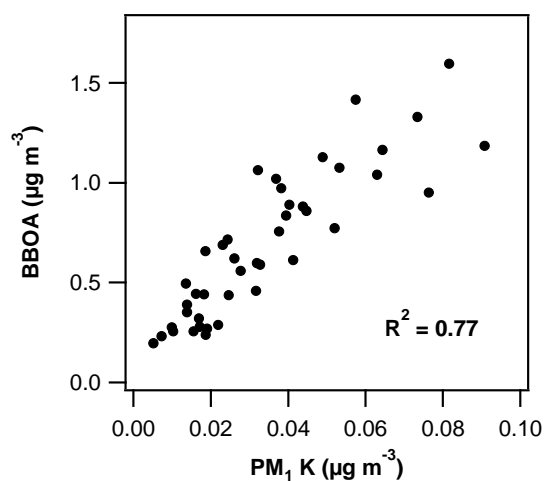


Figure S18. Contribution of BBOA in winter (averaged to 24-h periods matching the filter sampling) vs potassium concentrations in PM<sub>1</sub>.

Eliminado: 13

**Table S1. Squared Pearson correlation coefficients between OA sources/types and BC, sulphate, nitrate and ammonium for the warmer and the colder periods.**

	<b>R<sup>2</sup></b>	<b>BC</b>	<b>SO<sub>4</sub></b>	<b>NO<sub>3</sub></b>	<b>NH<sub>4</sub></b>
<b>Warmer period</b>	<b>HOA</b>	<b>0.51</b>	<b>0.16</b>	<b>0.23</b>	<b>0.16</b>
	<b>SV-OOA</b>	<b>0.32</b>	<b>0.17</b>	<b>0.16</b>	<b>0.13</b>
	<b>LV-OOA</b>	<b>0.45</b>	<b>0.34</b>	<b>0.27</b>	<b>0.43</b>
<b>Colder period</b>	<b>HOA</b>	<b>0.70</b>	<b>0.20</b>	<b>0.53</b>	<b>0.49</b>
	<b>BBOA</b>	<b>0.66</b>	<b>0.21</b>	<b>0.49</b>	<b>0.47</b>
	<b>OOA</b>	<b>0.71</b>	<b>0.49</b>	<b>0.73</b>	<b>0.79</b>

Tabla con formato

Eliminado: ¶

## REFERENCES

Eliminado: ¶

Crippa, M., DeCarlo, P. F., Slowik, J. G., Mohr, C., Heringa, M. F., Chirico, R., Poulain, L., Freutel, F., Sciare, J., Cozic, J., Di Marco, C. F., Elsasser, M., Nicolas, J. B., Marchand, N., Abidi, E., Wiedensohler, A., Drewnick, F., Schneider, J., Borrmann, S., Nemitz, E., Zimmermann, R., Jaffrezou, J. L., Prévôt, A. S. H., and Baltensperger, U.: Wintertime aerosol chemical composition and source apportionment of the organic fraction in the metropolitan area of Paris, Atmos. Chem. Phys., 13, 961-981, 10.5194/acp-13-961-2013, 2013.

Cubison, M. J., Ortega, A. M., Hayes, P. L., Farmer, D. K., Day, D., Lechner, M. J., Brune, W. H., Apel, E., Diskin, G. S., Fisher, J. A., Fuelberg, H. E., Hecobian, A., Knapp, D. J., Mikoviny, T., Riener, D., Sachse, G. W., Sessions, W., Weber, R. J., Weinheimer, A. J., Wisthaler, A., and Jimenez, J. L.: Effects of aging on organic aerosol from open biomass burning smoke in aircraft and laboratory studies, Atmos. Chem. Phys., 11, 12049-12064, 2011.

Middlebrook, A. M., Bahreini, R., Jimenez, J. L., and Canagaratna, M. R.: Evaluation of composition-dependent collection efficiencies for the Aerodyne aerosol mass spectrometer using field data, Aerosol Sci. Technol., 46, 258-271, 2012.

Minguillón, M. C., Perron, N., Querol, X., Szidat, S., Fahrni, S. M., Alastuey, A., Jimenez, J. L., Mohr, C., Ortega, A. M., Day, D. A., Lanz, V. A., Wacker, L., Reche, C., Cusack, M., Amato, F., Kiss, G., Hoffer, A., Decesari, S., Moretti, F., Hillamo, R., Teinilä, K., Seco, R., Peñuelas, J., Metzger, A., Schallhart, S., Müller, M., Hansel, A., Burkhardt, J. F., Baltensperger, U., and Prévôt, A. S. H.: Fossil versus contemporary sources of fine elemental and organic carbonaceous particulate matter during the DAURE campaign in Northeast Spain, Atmos. Chem. Phys., 11, 12067-12084, 10.5194/acp-11-12067-2011, 2011.

Ng, N. L., Canagaratna, M. R., Jimenez, J. L., Zhang, Q., Ulbrich, I. M., and Worsnop, D. R.: Real-time methods for estimating organic component mass concentrations from aerosol mass spectrometer data, Environ. Sci. Technol., 45, 910-916, 2011.